

Article

Observed Changes in Crop Yield Associated with Droughts Propagation via Natural and Human-Disturbed Agro-Ecological Zones of Pakistan

Farhan Saleem ^{1,2,†}, Arfan Arshad ^{3,4,†}, Ali Mirchi ³, Tasneem Khaliq ⁵, Xiaodong Zeng ^{1,2,6,*}, Md Masudur Rahman ⁷, Adil Dilawar ^{2,8}, Quoc Bao Pham ⁹ and Kashif Mahmood ¹⁰

¹ International Center for Climate and Environment Sciences, Institute of Atmospheric Physics, Chinese Academy of Sciences, Beijing 100029, China; farhan@mail.iap.ac.cn

² University of Chinese Academy of Sciences, Beijing 100049, China; adilawar2018@igsnr.ac.cn

³ Department of Biosystems and Agricultural Engineering, Oklahoma State University, Stillwater, OK 74078, USA; arshad@okstate.edu (A.A.); amirchi@okstate.edu (A.M.)

⁴ Department of Irrigation and Drainage, Faculty of Agricultural Engineering, University of Agriculture Faisalabad, Faisalabad 38000, Pakistan

⁵ Agro-Climatology Laboratory, Department of Agronomy, University of Agriculture, Faisalabad 38000, Pakistan; drtasneem@uaf.edu.pk

⁶ Collaborative Innovation Center on Forecast and Evaluation of Meteorological Disasters, Nanjing University of Information Science and Technology, Nanjing 210044, China

⁷ Department of Electrical and Electronic Engineering, Pabna University of Science & Technology, Pabna 6600, Bangladesh; mmrahman@pust.ac.bd

⁸ State Key Laboratory of Resources and Environmental Information System, Institute of Geographic Sciences and Natural Resources Research, Chinese Academy of Sciences, Beijing 100029, China

⁹ Institute of Applied Technology, Thu Dau Mot University, Thu Dau Mot 820000, Vietnam; phambaoquoc@tdmu.edu.vn

¹⁰ Center for Development Research (ZEF), University of Bonn, 53113 Bonn, Germany; kashif.mehmood@uni-bonn.de

* Correspondence: xdzeng@mail.iap.ac.cn

† These authors contributed equally to this paper.

Citation: Saleem, F.; Arshad, A.; Mirchi, A.; Khaliq, T.; Zeng, X.; Rahman, M.M.; Dilawar, A.; Pham, Q.B.; Mahmood, K. Observed Changes in Crop Yield Associated with Droughts Propagation via Natural and Human-Disturbed Agro-Ecological Zones of Pakistan. *Remote Sens.* **2022**, *14*, 2152. <https://doi.org/10.3390/rs14092152>

Academic Editor: John J. Qu

Received: 11 March 2022

Accepted: 26 April 2022

Published: 30 April 2022

Publisher's Note: MDPI stays neutral with regard to jurisdictional claims in published maps and institutional affiliations.



Copyright: © 2022 by the authors. Licensee MDPI, Basel, Switzerland. This article is an open access article distributed under the terms and conditions of the Creative Commons Attribution (CC BY) license (<https://creativecommons.org/licenses/by/4.0/>).

Abstract: Pakistan's agriculture and food production account for 27% of its overall gross domestic product (GDP). Despite ongoing advances in technology and crop varieties, an imbalance between water availability and demand, combined with robust shifts in drought propagation has negatively affected the agro-ecosystem and environmental conditions. In this study, we examined hydro-meteorological drought propagation and its associated impacts on crop yield across natural and human-disturbed agro-ecological zones (AEZs) in Pakistan. Multisource datasets (i.e., ground observations, reanalysis, and satellites) were used to characterize the most extensive, intense drought episodes from 1981 to 2018 based on the standardized precipitation evaporation index (SPEI), standardized streamflow index (SSFI), standardized surface water storage index (SSWSI), and standardized groundwater storage index (SGWI). The most common and intense drought episodes characterized by SPEI, SSFI, SSWSI, and SGWI were observed in years 1981–1983, 2000–2003, 2005, and 2018. SPEI yielded the maximum number of drought months (90) followed by SSFI (85), SSWSI (75), and SGWI (35). Droughts were frequently longer and had a slower termination rate in the human-disturbed AEZs (e.g., North Irrigated Plain and South Irrigated Plain) compared to natural zones (e.g., Wet Mountains and Northern Dry Mountains). The historical droughts are likely caused by the anomalous large-scale patterns of geopotential height, near-surface air temperature, total precipitation, and prevailing soil moisture conditions. The negative values (<-2) of standardized drought severity index (DSI) observed during the drought episodes (1988, 2000, and 2002) indicated a decline in vegetation growth and yield of major crops such as sugarcane, maize, wheat, cotton, and rice. A large number of low-yield years ($\text{SYRI} \leq -1.5$) were recorded for sugarcane and maize (10 years), followed by rice (9 years), wheat (8 years), and cotton (6 years). Maximum crop yield reductions relative to the historic mean (1981–2017) were recorded in 1983 (38% for cotton), 1985

(51% for maize), 1999 (15% for wheat), 2000 (29% for cotton), 2001 (37% for rice), 2002 (21% for rice), and 2004 (32% for maize). The percentage yield losses associated with shifts in SSFI and SWSI were greater than those in SPEI, likely due to longer drought termination duration and a slower termination rate in the human-disturbed AEZs. The study's findings will assist policymakers to adopt sustainable agricultural and water management practices, and make climate change adaptation plans to mitigate drought impacts in the study region.

Keywords: spatiotemporal droughts; termination; GRACE; crop yield sensitivity; atmospheric circulation; Pakistan

1. Introduction

Droughts are among the most prevalent hydro-meteorological hazards [1], affecting agricultural productivity [2,3], water resources [4], the ecosystem [5], and the environment [6], with significant impacts on the economy at local and global scales [7]. It is often challenging to detect and predict the start and areal extent of droughts because of their complex nature and non-structural impacts [8,9]. An increase in drought events has been reported worldwide [10–15] and droughts are expected to become more frequent and intense in the near future [16]. The robust shifts in extreme high temperatures [17] make water-scarce regions of the world more vulnerable to drought risks [18].

Comprehensive and timely information about the spatiotemporal extent of droughts (i.e., intensity and frequency) is needed to mitigate drought impacts [19–21]. The significant effects of extreme high temperatures on global agriculture are well documented in the literature [22]. Concurrent spells of heatwave and drought have caused considerable loss of food crops in Europe [23]. Prolonged growing seasons in a warming world increase the evapotranspiration rate and decrease soil moisture, which, in turn, contribute to a higher risk of flash droughts [24]. Famines related to hot (dry) weather extremes can result in vegetation die-off, negatively impacting agronomic practices [25]. A study reported a 10% drop in rice yield due to a 1 °C increase in nighttime extreme temperatures [26]. Climate variability and trends were found to be uneven between the means and daytime (nighttime) extremes [27]. The warming signal is already evident with no uniform pattern throughout the globe [16,28]. For instance, the estimated global warming rate was 0.74 °C during 1906–2005, and regional warming reached from 0.4 to 0.8 °C [27].

Inconsistent monsoon patterns over the South Asian domain, including Pakistan, will negatively impact agroecosystems over the 21st century [29,30]. Pakistan is a predominantly arid/semi-arid country with an agriculture-dependent economy [31]. Climate extremes have adversely affected the region's environmental conditions [17,32]. The southern and central parts of Pakistan experienced more frequent dry spells due to stable higher temperature and interannual rainfall variability, in turn, affecting the agriculture and water resources [18,33,34]. In the recent decade, groundwater has become the second largest source of water for irrigated agriculture in Pakistan, contributing 22% to gross domestic product (GDP) and helping meet 45% of crop water requirements [33,35,36]. The water table in the Baluchistan and Sindh provinces has declined substantially due to groundwater overdraft [37]. The surface water storage capacity of Mangla, Tarbela, and Chashma reservoirs decreased by 30% due to siltation and climate change [38], increasing the risk of water scarcity compared to the historical mean [39]. The region has experienced moderate to severe water shortages, driven mainly by drought and intensive irrigation [40]. The historic dry spells (1999–2002) resulted in the crop yield loss of rain-fed and irrigated crops by 80% and up to 20%, respectively, with extensive impacts on the GDP of Pakistan [41,42].

Previous efforts have investigated historical changes in droughts over South Asia (SA), including Pakistan, based on the standardized precipitation index (SPI) and the

standardized precipitation evapotranspiration index (SPEI) using precipitation, soil moisture, land surface, and air temperature [18,43–49]. However, research gaps remain in accounting for the hydrological factors (e.g., surface water storage (SWS), groundwater storage (GWS), and stream flow (SF)) directly influencing the surface and sub-surface water cycle. Further, the spatial variability of extreme hydro-climatic conditions over the natural and human-disturbed agro-ecological zones (AEZs) of Pakistan remains unknown. A detailed description of AEZs and their salient features are given in [17]. Recent studies have demonstrated that surface and sub-surface water storage in the study region have declined in recent years due to climate dynamics mainly induced by El Niño Southern Oscillation (ENSO), in addition to anthropogenic depletion to meet the growing water and food demands [50–53]. The standardized stream flow index (SSFI) [54], standardized groundwater storage index (SGWI) [55] and standardized surface water storage index (SWSI) [56] work similarly to traditional drought indices (e.g., standardized precipitation index (SPI)); however, these indicators provide a more in-depth understanding of the hydrological cycle.

The objective of this study was to characterize the historic long-term variability of extreme hydro-climatic conditions and their influences on crop production over natural and human-disturbed AEZs of Pakistan through a variety of hydro-meteorological and agricultural drought indices (i.e., SPEI, SSFI, SGWI, SWSI, and DSI). Drought events (e.g., duration, rate, and intensity) and termination (timing of the recovery of drought events) characteristics vary depending on natural (water transfer) and human-disturbed (water abstractions) regions [57], and affect the agro-system to different extents [58]. Drought termination is a point when a drought is said to have ended with a quantifiable event in a temporal profile [59]. Drought effects (e.g., duration, rate, and intensity) have been widely studied by different researchers in the study region [47–49]; however, feedback of drought termination through the hydro-meteorological cycle is still poorly understood in the study region. Therefore, an understanding of how and when a drought is likely to terminate and its ultimate influences on the agro-ecosystem is crucial for water management and decision-making processes. In the present study, the influences of a series of hydro-climate indicators on crop production were explored through yield sensitivity analysis [60] and yield losses using the empirical relationships [58,61]. We discuss long-term changes in hydro-meteorological conditions using drought events and termination characteristics. The paper improves understanding of the long-term historical changes in major crop yields, providing insights into the sensitivity of each crop's yield to changes in hydro-meteorological drought indices across different AEZs.

2. Materials and Methods

2.1. Study Area

The study area lies between the latitudes of 23–37° North and longitudes of 60–77° East, covering 10 different AEZs over a landmass of ~796, 100 km² in Pakistan (Figure 1a). The Indus river and its main tributaries (Indus, Jhelum, Chenab, Ravi, Beas, and Sutlej) are the major source of surface water, which flows downstream towards the Arabian Ocean. The elevation in the study region changes from a minimum of 10 m in the south to a maximum of 8000 m in the northern high-mountain regions. The annual precipitation varies from a minimum of 50–600 mm/year in the downstream zones to a maximum of 1800 mm/year in the upstream regions (Figure 1b). The Barani-Rainfed agricultural region receives higher precipitation compared to other zones. The average irrigation supply varies, with downstream regions relying primarily on surface water and upstream regions relying primarily on groundwater irrigation (Figure 1c,d). The principal crops are wheat, sugarcane, cotton, rice, and maize, with different cropping calendars and two major cropping seasons, namely Rabi and Kharif (Figure S1). Based on complex topographical, agricultural, water transfer, and utilization characteristics, the AEZs in study region are fur-

ther characterized into natural and human-disturbed regions (Table S1 in the Supplementary file). Most headwater zones are categorized as natural due to their water transfer characteristics, whereas mid and downstream zones are human-disturbed, which are regulated by human abstractions. Table S1 lists the geographic and hydrological information and dominant activities across each zone.

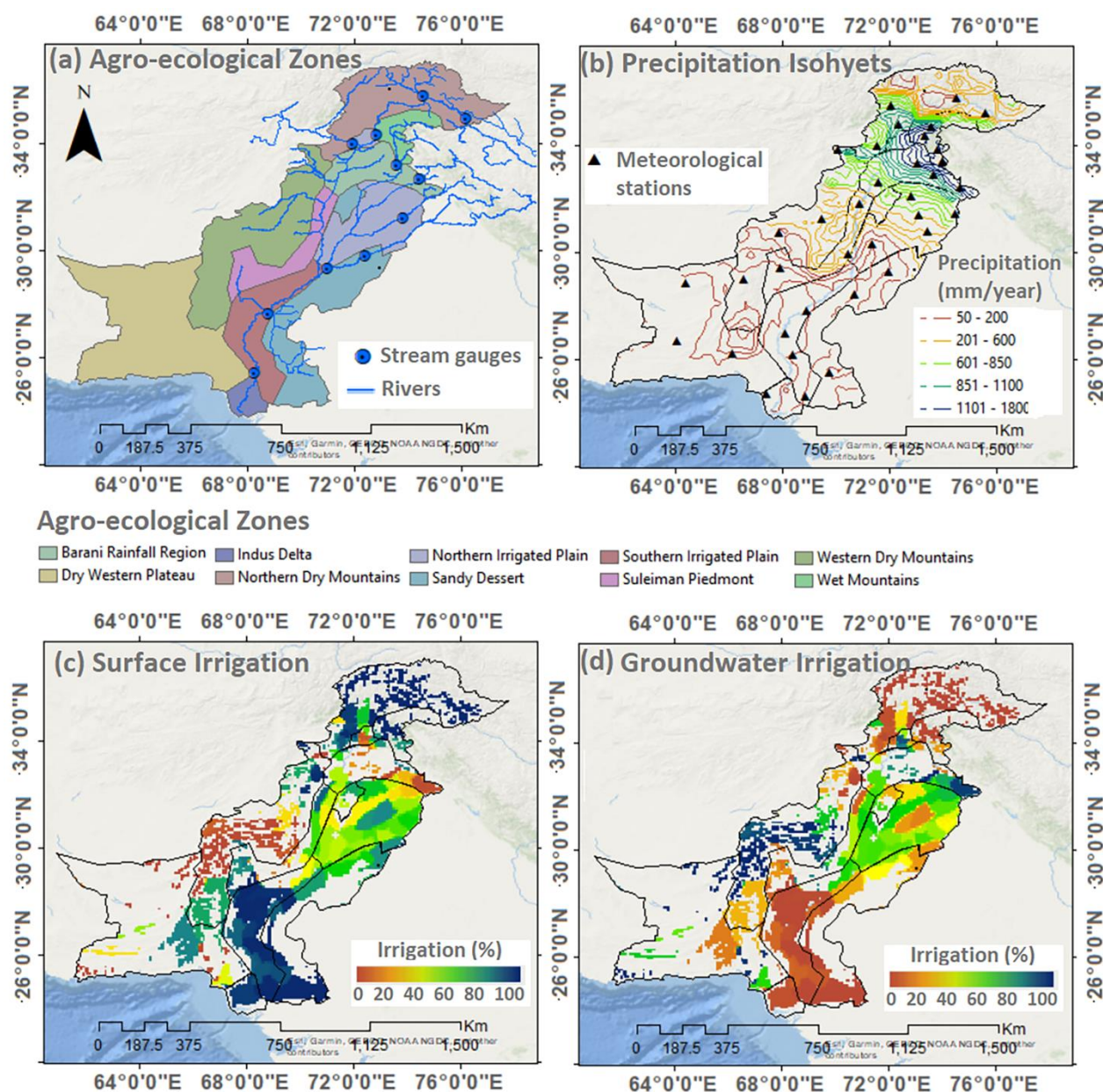


Figure 1. Map of the study area showing (a) geographical location of stream gauges, river networks, and 10 different AEZs, (b) meteorological stations and precipitation isohyets, (c) % irrigation with surface water, and (d) % irrigation with groundwater.

2.2. Data Collection and Preprocessing

We used a combination of data sources, such as in situ observations, satellite datasets, a land surface model (LSM), and reanalysis.

In situ observation data: Daily time series of temperature (T_{max} , T_{min}) and precipitation from 38 meteorological stations scattered over different AEZs were obtained from Pakistan Meteorological Department (PMD) from 1981 to 2019. Daily streamflow data from 14 gauges were obtained from Pakistan Water and Power Development Authority

(WAPDA), of which 10 stations had data from 1981–2018, whereas the remaining four stations had a shorter streamflow record (1994–2018). Crop yield time-series data (1981–2017) for five main crops (sugarcane, wheat, cotton, rice, and maize) were collected from Pakistan’s Agriculture Marketing Information Service (AMIS), which curates data across 122 districts in the study region. In situ observation data of the depth to water table (DTWT) for 1674 observational wells were collected from Punjab Irrigation Department PID, Lahore, Pakistan (<https://irrigation.punjab.gov.pk/>, 13 March, 2021).

Land surface model (LSM) and reanalysis output: High-resolution monthly actual evapotranspiration (ET_a) data of the reanalysis product (Terra-Climate) at a spatial resolution of 0.04° grid was collected from the Climatology Lab (<http://www.climatologylab.org/terraclimate.html>, 13 March, 2021) covering the period of 1981–2018. These data provide an important input for eco-hydrological and meteorological applications at a scale. Monthly terrestrial water storage (TWS) output data of the land surface model (LSM) were taken from GLDAS (Global Land Data Assimilation System) version CLSMv2.0 for the period 1981–2018 with a spatial resolution of $0.25^\circ \times 0.25^\circ$ (<https://disc.gsfc.nasa.gov/datasets>, 13 March, 2021). GLDAS TWS comprises different surface storage compartments, such as soil moisture storage (SMS), surface runoff (Qs) canopy water storage (CWS), and snow water equivalent (SWE). GLDAS data have been widely applied by different researchers to investigate the water storage variations in the study region [50,62–64].

Satellite Data: Normalized difference vegetation index (NDVI) data were prepared from Landsat data. Satellite imageries of RED and NIR bands were taken from Landsat 5 Thematic Mapper (TM) and Landsat 8 (Operational Land Imager (OLI) at a spatial (temporal) resolution of 30 m (16 days) for the period of 1985–2018 (<http://earthexplorer.usgs.gov/>, 13 March, 2021). Spectral reflectance of NIR and RED bands was used to compute the normalized difference vegetation index (NDVI), as follows (see details in Supplementary file);

$$NDVI = \frac{NIR - RED}{NIR + RED} \quad (1)$$

NDVI values range between -1 and 1 . The closer the values of the NDVI index to 1 , the higher the density of green vegetation. NDVI values near 0 indicate non-vegetated areas and negative values indicate water.

Gravity Recovery and Climate Experiments (GRACE) satellites provided the terrestrial water storage anomalies (TWSA) data, which comprise surface and sub-surface storage compartments, such as surface water, soil moisture, snow, ice, groundwater, and biomass [65]. Monthly GRACE-based terrestrial water storage anomalies (TWSA) of the Mascon solution were obtained from 2002–2018 at a $0.5^\circ \times 0.5^\circ$ resolution (<http://www2.csr.utexas.edu/grace/>, 13 March, 2021). GLDAS-based surface water storage compartments (soil moisture storage (SMS), surface runoff (Qs) canopy water storage (CWS), and snow water equivalent (SWE)) were subtracted from the GRACE-based TWSA data to obtain the groundwater storage anomalies (GWSAs) using the following expression:

$$GWSA = TWSA_{GRACE} - (\Delta SMS + \Delta Qs + \Delta CWS + \Delta SWE)_{GLDAS} \quad (2)$$

where ΔSMS , ΔQs , ΔCWS , and ΔSWE represent the anomalies of SMS, Qs, CWS, and SWE, respectively, which were obtained by subtracting the long-term mean (2004–2009) from the monthly data, in the same manner as for the GRACE-based TWSA [62]. GRACE-based GWSAs were validated with observational data. Groundwater data from observational wells are available in the form of the depth to water table (DTWT), which was converted into groundwater storage anomalies (GWSAs) using the following expression:

$$GWS = (DTB - DTWT) \times S_y \quad (3)$$

where GWS represents the groundwater storage (GWS), DTB is the depth to bedrock (average DTB for study area = 400 m [50]), and S_y is the specific yield of aquifer (average specific yield for the study area is 0.12 [50,66]). Finally, GWS was converted to anomalies (GWSAs) by subtracting the long-term mean (2004–2009, as for the GRACE data). GRACE-based GWSAs show a similar change as estimated from ground-based observation data with reasonable accuracy (R^2 range: 0.68–81) (see Figure S2 in Supplementary file). Previous studies have also found that GRACE-based GWSAs provide reasonable accuracy to track water storage variations when compared with observational data in the study area [50,63,64,67].

2.3. Quantification of Hydro-Meteorological and Agricultural Droughts

We evaluated the extreme hydro-meteorological conditions based on several drought characteristics, such as drought events (months, duration, frequency, intensity) and drought termination (termination duration and rate) (Table 1). The quantification of each drought indicator is described below.

Table 1. Summary of drought event and termination characteristics.

Characteristics		Description
Drought event	Duration (D)	The sum of durations (d) for all drought events divided by the number of drought events (n): $D = \frac{\sum_{j=1}^n d}{n}$
	Frequency (D_{freq})	The ratio between the number of drought months (n_m) and the total number of drought months (N_m) in the time series: $D_{freq} = (n_m/N_m) \times 100$
	Drought Magnitude (DM)	The sum of values for all drought spells is referred to as DM.
	Intensity (I)	The ratio between drought magnitude and duration: $I = \frac{DM}{D}$
Drought termination	Maximum Intensity (MI)	Difference between peak values of drought and threshold value
	Drought termination start (DT_{start})	Onset of the drought termination phase, or the month in which the maximum intensity (MI) is reached.
	Drought termination end (DT_{end})	Last month of the drought termination phase
	Drought termination duration (DT_{dur})	Number of months between DT_{start} and DT_{end} for each drought event.

Meteorological droughts: The standardized precipitation and evaporation index (SPEI) was used to investigate changes in meteorological extremes. The SPEI uses precipitation (P_i) and potential evapotranspiration (PET_i) in drought characterization. P_i and PET_i were used to calculate the monthly water deficit (WD_i):

$$WD_i = P_i - PET_i \quad (4)$$

Due to the limitations of climate parameters, PET was computed using the Hargreaves method [68], which uses T_{max} , T_{min} , and R_a (altitude dependent extraterrestrial radiation). PET is calculated as follows:

$$PET = 0.0023 \times R_a \times (T_{max} - T_{min})^{0.5} (T_{mean} + 0.5) \quad (5)$$

WD_i results were fed into the SPEI R-package to calculate the SPEI at different time-scales (<http://cran.r-project.org/web/packages/SPEI>, 13 March, 2021). The SPEI time series was derived using Equation (6):

$$f(x) = \left[1 + \left(\frac{\alpha}{x - \gamma} \right)^\beta \right]^{-1} \quad (6)$$

where α , β , and γ are the scale, shape, and origin parameters, respectively.

$$\text{SPEI} = W - \frac{c_0 + c_1W + c_2W^2}{1 + d_1W + d_2W^2 + d_3W^3} \quad (7)$$

$$W = \sqrt{-2 \ln(P)} \quad (8)$$

when $P \leq 0.5$, $P = 1 - f(x)$; when $P > 0.5$, $P = 1 - P$, and the sign of the SPEI is inverted. $c_0 = 2.515517$, $c_1 = 0.802853$, $c_2 = 0.010328$, $d_1 = 1.432788$, $d_2 = 0.189269$, and $d_3 = 0.001308$ are constants. The regional SPEI in each AEZ was obtained by averaging climate data of all stations located in that zone. The SPEI time series provides positive and negative values, which represent the wet and dry conditions, respectively. The detailed criteria of various drought classes (i.e., mild, moderate, severe, and extreme droughts) are given in [69]. The threshold value of -1 ($\text{SPEI} \leq -1$) was used to determine the drought condition.

Hydrological droughts: The standardized streamflow index (SSFI), standardized surface water storage index (SSWSI), and standardized groundwater storage index (SGWI) were used to capture the hydrological conditions in natural and human-disturbed AEZs. SSFI is based on the long-term time-series record of streamflow observations. SSFI for a given period is calculated as the difference in the streamflow from the mean divided by the standard deviation (Equation (9)).

$$\text{SSFI} = \frac{y_i - \mu}{\sigma} \quad (9)$$

where y_i is the original times series values of streamflow at time i , μ is the long-term mean of streamflow, and σ is the standard deviation. SSWSI and SGWI indicators were statistically calculated similarly to SSFI. However, the SSWSI time series comprises soil moisture storage (SM), canopy water storage (CWS), snow water equivalent (SWE), and runoff as input parameters, and SGWI involves the GRACE-based groundwater storage anomaly (GWSA) as the input parameter. The time series of hydrological droughts (SSFI, SSWSI, and SGWI) exhibits positive and negative values representing the wet and dry conditions. SSFI, SSWSI, and SGWI time series were computed at different timescales, similar to SPEI. The use of a shorter timeframe, such as six months, is recommended for agricultural drought monitoring [70,71]. Recent studies on the linkage between drought indices and agricultural impacts also indicate that the six-month (i.e., SPEI-6) index is adequate for evaluating drought impacts on agriculture [71–73]. Therefore, SPEI and other drought indices spanning six months were adopted for further analysis.

Agricultural droughts: We also computed the Landsat-based drought severity index (DSI) using NDVI and ET/PET to quantify agricultural droughts as a proxy for vegetation and biomass changes. Computation of the DSI was undertaken in three steps: (1) standardization of the NDVI and ET/PET, (2) summation of the standardized NDVI and ET/PET to obtain the Z value, and (3) standardization of the Z value to obtain the DSI [74] as follows:

$$Z_{NDVI} = \frac{NDVI - \overline{NDVI}}{\sigma} \quad (10)$$

$$Z_{\frac{ET}{PET}} = \frac{\frac{ET}{PET} - \overline{\frac{ET}{PET}}}{\sigma} \quad (11)$$

$$Z = Z_{NDVI} + Z_{\frac{ET}{PET}} \quad (12)$$

$$\text{DSI} = \frac{Z - \overline{Z}}{\sigma} \quad (13)$$

Positive DSI values indicate wet/favorable conditions for vegetation growth, whereas negative values indicate dry/drought conditions, i.e., vegetation stress.

2.4. Composite Analysis

The relationships between large scale circulation patterns and historic drought episodes were explored using composite analysis. This approach has been widely used to determine the response of a variable to particular event [47]. The ERA5 monthly reanalysis data (1981–2018) with a horizontal resolution of 0.25° grid were used for compositing. The single and multi-level meteorological fields chosen as possible drivers of historic droughts were two-meter air temperature, total precipitation, 850 mb relative humidity, 500 hPa geopotential height, soil moisture, and soil temperature.

2.5. Standardized Crop Yield Estimation

Crop production in the region has an overall increasing trend due to advances in technology and adaptation practices in agricultural sectors [58,75]. Therefore, we used a linear regression method to remove the technological effect from the yield [76]. The residual yield $y_i^{(T)}$ was calculated using Equation (14).

$$y_i^{(T)} = y_i^0 - y_i^{(\tau)} \quad (14)$$

where y_i^0 is the observed crop yield and $y_i^{(\tau)}$ is the value of the detrended yield. The effects of climate on crop yield are expressed by the residuals [58,77]. We subsequently derived the standardized yield residual index (SYRI):

$$SYRI = \frac{y_i^{(T)} - \mu}{\sigma} \quad (15)$$

where $y_i^{(T)}$ is the residual of the detrended yield, μ is the mean of the detrended yield residuals, and σ is the standard deviation. Negative values in the SYRI time series reflect a decrease in crop yield compared to the long-term average.

2.6. Calculation of Crop Yield Sensitivity and Yield Losses

We calculated the yield sensitivity of each crop by establishing a statistical relationship between crop production and seasonal anomalies of hydro-meteorological indicators (streamflow, groundwater storage (GWS), surface water storage (SWS), and precipitation). For a given year, anomalies for each indicator were calculated by dividing each indicator's long-term average value in the growing season by the actual amount of water in the same period. Similarly, the yield anomaly index was calculated as a measure of the yield's deviation from the normal. Finally, the yield sensitivity index for each crop was calculated by dividing the yield anomaly index by the anomalies of hydro-meteorological indicators [60]. The sensitivity index value becomes larger if there is a high yield value change with a small change in hydro-meteorological indicators, and vice versa. Furthermore, we used empirical relationships among crop yields and hydro-meteorological drought indices to estimate the yield losses (%) of wheat, cotton, sugarcane, maize, and rice from 1981 to 2017 [58,61]. The yield losses (%) for each crop were determined by dividing the annual crop yield by the dynamically averaged yield value of the quadratic trend and multiplying the resulting ratio by 100 [78].

3. Results

3.1. Historical Trend in Hydro-Meteorological Droughts

The spatial pattern of droughts derived from SPEI at a six-month timescale (SPEI-6) reveals an increasing trend, mostly over the human-disturbed AEZ's in Southern Pakistan (Figure 2). In contrast, a slightly decreasing trend is apparent in Central and Northern AEZs. These findings are consistent with previous studies conducted in the South Asian domain [32,79,80]. Time-series changes in SPEI-6 index show mild to extreme drought conditions in various AEZs. The drought episodes display a uniform pattern in some AEZs; however, predominantly non-uniform patterns have been observed among most

AEZs, likely due to heterogeneity in climate conditions in each region [17]. The interannual rainfall variability and temperature are the primary factors of meteorological droughts in SA [81]. For instance, 1986, 1988, 2001, 2002, 2009, and 2018 were distinctly marked as mild to moderate drought years for the Wet Mountains zone, which generally receives a high amount of annual rainfall (~1200–1600 mm/year), whereas 1981, 1982, 1983, 2000–2003, 2005 and 2018 were highlighted as moderate to severe and extreme drought periods for the Dry Western Plateau, which receives the lowest amount of rainfall (~100–200 mm/year). Notably, arid to semi-arid zones (i.e., Western Dry Mountains, Dry Western Plateau) experienced higher numbers of drought episodes, indicating that these areas are more vulnerable to drought [18,82]. The historic drought episodes have affected 150 million people in the African Sahel, 83 million in China, and 19 million in Australia [79]. The intensity of La Niña and ENSO episodes (particularly between 1998 and 2003) significantly impacted climate extremes in terms of climate variability and transition across SA [30,33].

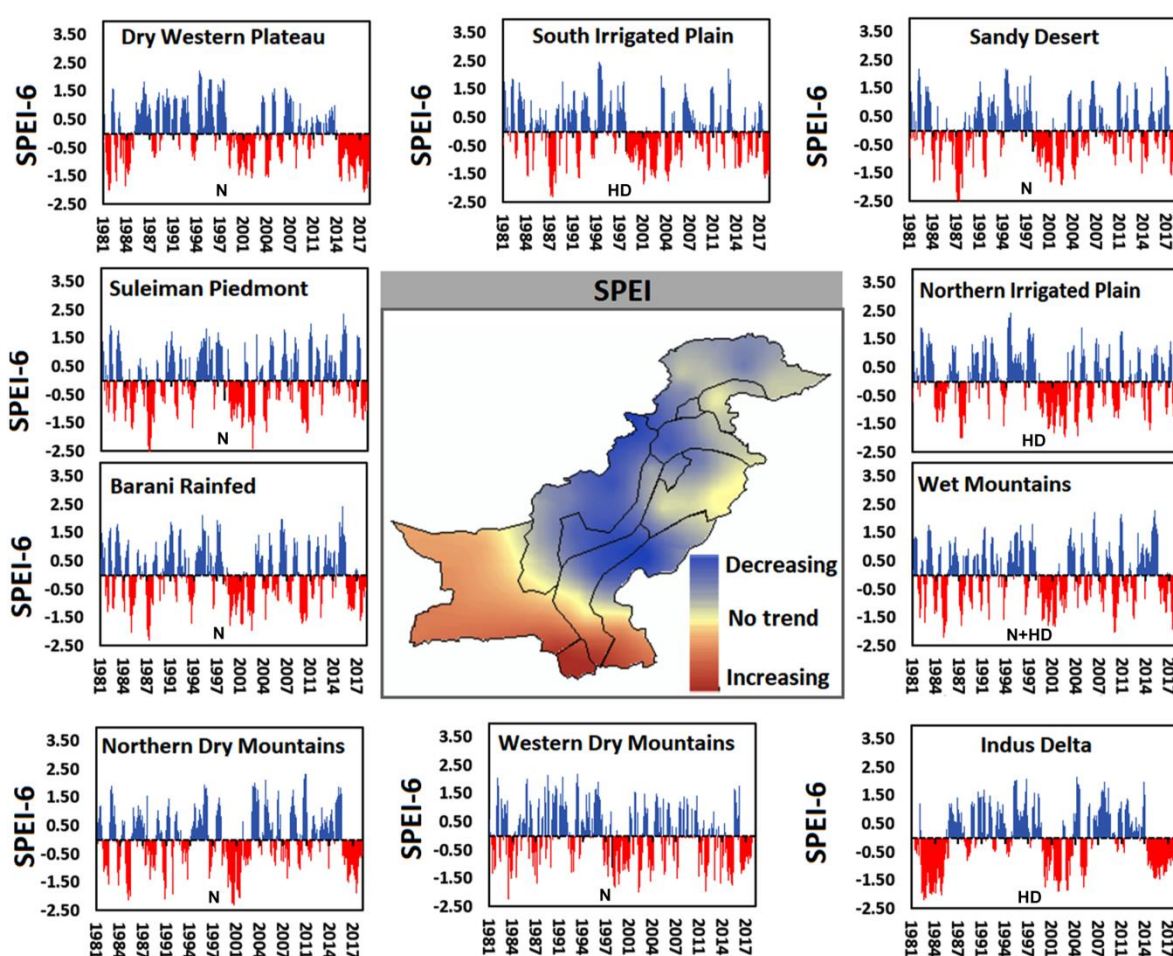
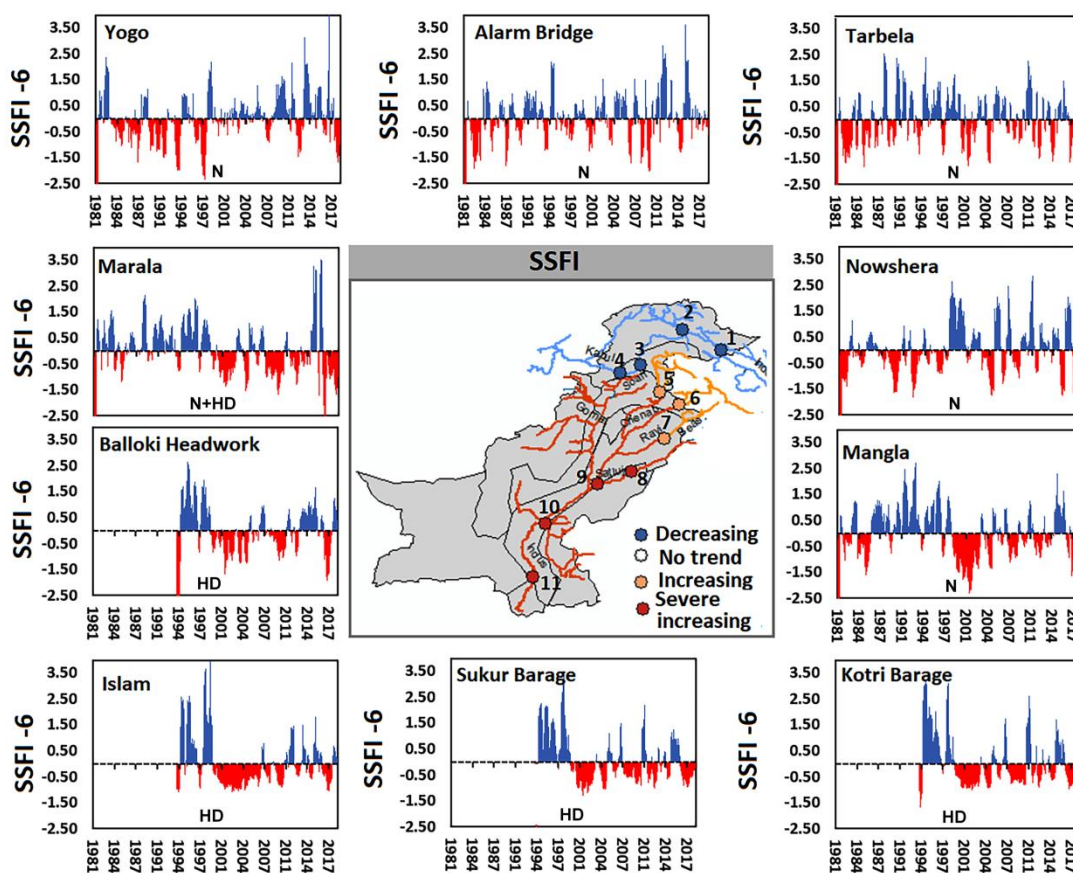


Figure 2. Spatial trend and time series of the standardized precipitation evaporation index at a six-month timescale (SPEI-6) over different AEZs. Note: N and HD represent natural and human-disturb zones, respectively.

Figure 3 depicts the long-term spatial trend and time-series variations of SSFI-6 for 10 stream gauges located in different AEZs. The SSFI data are unavailable for some zones (such as Suleiman Piedmont, Dry Western Plateau, and Western Dry Mountains) due to the lack of a stream network or observed records. The long-term (1981–2017) spatial trends of SSFI indicated an obvious increase in droughts for downstream gauge stations located across human-disturbed AEZs (Figure 3), whereas the reverse patterns are seen for up-

stream gauge stations located in the natural zones. The upstream stations are mostly located over the core monsoon zone, which receives adequate rainfall during the summer monsoon and winter rainfall in the form of snow [83]. In addition, the influence of urbanization and land-use patterns on streamflow variability is also evident in the literature [84]. Drought episodes detected by SSFI overlapped with drought episodes observed with SPEI for some years. Overall, extensive dry events occurred in 2001–2003, whereas most of the selected stream gauging stations registered wet events in 1994–1996. Interestingly, SSFI time series for the Yogo, Terbela, Nowshera, and Mangla stream gauge stations located in the natural zones (e.g., Wet Mountains and Northern Dry Mountains) depicted less frequent drought episodes. However, the historical trend of SSFI over human-disturbed stream gauging stations, such as Balloki Headwork (located in the Northern Irrigated Plain), Sukur Barrage (Southern Irrigated Plain), and Kotri Barrage (Indus Delta), showed continuous shifts from wet to dry conditions during 1981–2018, which is likely associated with a large diversion of surface water for irrigation supply in these zones [39,40]. This finding agrees with a hydrologic study (i.e., monthly mean streamflow and long-term trends) of the mountainous areas in northwestern Pakistan [85]. Human activities (i.e., water abstraction for surface irrigation) lower the streamflow regime and exacerbate hydrological droughts. Various studies further confirm water abstraction’s effects on streamflow droughts worldwide [86,87].



Stream Gauges

1-Yogo 2-Alarm Bridge 3-Tarbela 4-Nowshera 5-Mangla 6-Maral 7-Balloki 8-Islam 9-Panjnad 10-Sukkar 11-Kotri

Figure 3. Spatial trend and time series of standardized streamflow index at a 6-month timescale (SSFI-6) for 10 stream gauging stations located in the AEZs. Note: N and HD represent natural and human-disturb zones, respectively.

An increasing drought trend (spatial pattern) is apparent for the AEZs located towards southwestern and northeastern Pakistan (Figure 4). Drought events were highlighted based on the threshold value of SSWSI < -0.5. The spatial trend of droughts exhibited mixed patterns during 1981–2017. The southwestern, central, and northeastern zones are highly susceptible to drought risks because of the arid to semi-arid climate conditions [33]. These results are in good agreement with earlier studies on hydrological droughts [88,89]. Notably, the historical time series of droughts obtained from SSWSI-6 reflects drought events associated with SPEI-6 time-series variations over most AEZs. More frequent hydrological droughts based on SSWSI-6 were recorded for the years of 1981, 1985, 1989, 1993, 1999–2002, and 2017–2018. Since SSWSI was calculated as the sum of soil moisture, canopy water, and runoff, changes in SSWSI are more sensitive to any change in the precipitation cycle and climate variability. For instance, it can be seen that the time series of changes in SSWSI-6 across the Sandy Desert show a declining trend between 1984–1990 and 1998–2003, strongly associated with changes in precipitation extremes during this period [18]. Furthermore, the recent decrease in SSWSI-6 during drought episodes may also be linked to El Niño events [52].

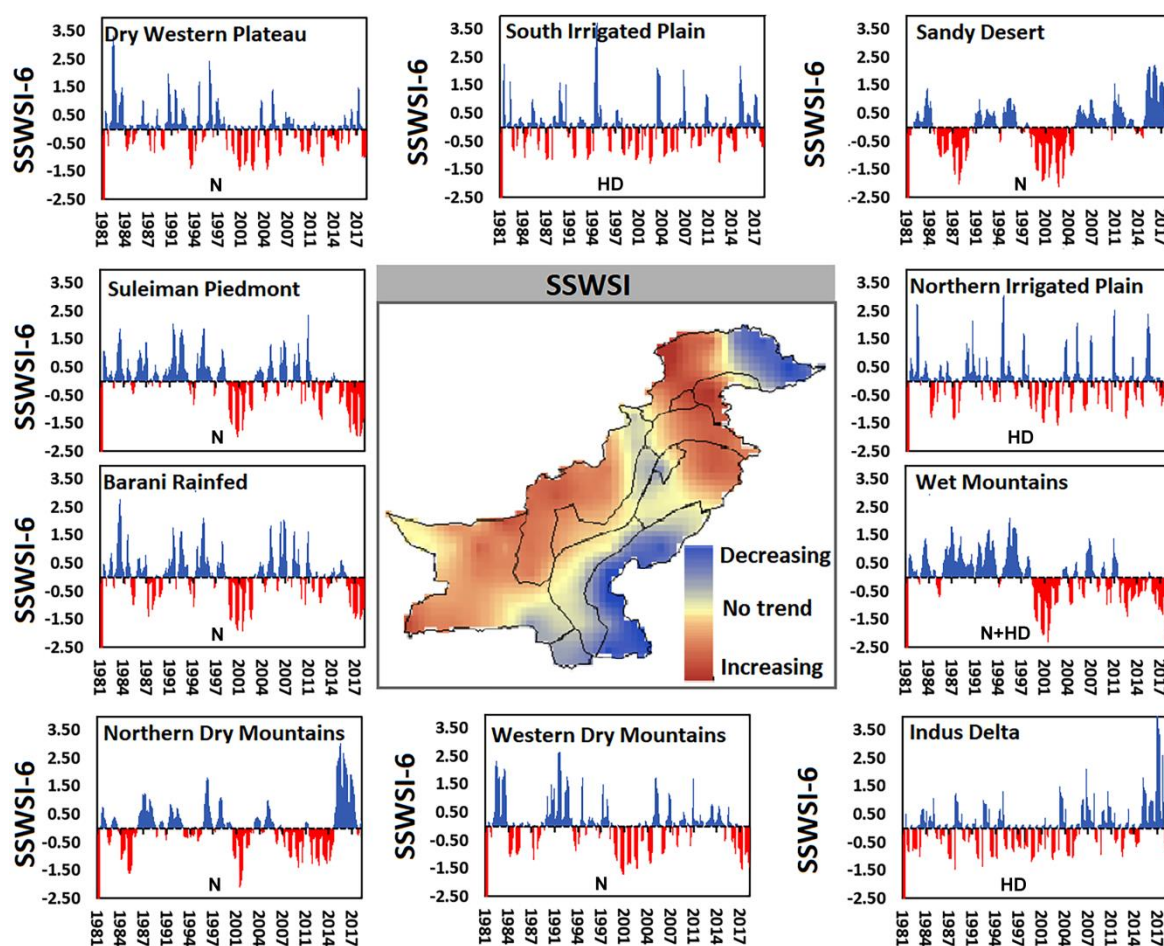


Figure 4. Spatial trend and time series of standardized surface water storage index at a 6-month timescale (SSWSI-6) for 10 different AEZs. Note: N and HD represent natural and human-disturb zones, respectively.

We also investigated the sub-surface hydrological droughts in terms of aquifer depletion using SGWI index at a 6-month timeframe (Figure 5). It is important to evaluate this index since groundwater is being depleted continuously to meet the demands of agriculture and population [36,37]. The spatial trend of SGWI index shows heterogeneity in drought patterns with an increasing trend observed in the North Irrigated Plain. Climate

and land-use patterns have significantly impacted the hydrological cycle in the Punjab province of Pakistan, reducing groundwater recharge by 15% [88]. The drying trend in groundwater in the Mediterranean and Eastern Europe regions has been associated with changes in land-use land cover patterns [90]. Most of the zones had drought episodes in recent years. However, drought episodes (i.e., during 2004, 2005, 2007, and 2011) were more frequent in human-disturbed zones (North Irrigated Plain) compared to other zones. Earlier studies also reported the sensitivity of groundwater drought to hydroclimatic conditions, where anthropogenic activities had a larger effect on groundwater recharge than climate change [88,90,91]. All AEZs except Barani-Rainfed and Wet Mountains show a continuous decline in groundwater storage and a shift from wetter to drier conditions during 2002–2018, which is probably associated with a large abstraction of groundwater for irrigation supply [35,37].

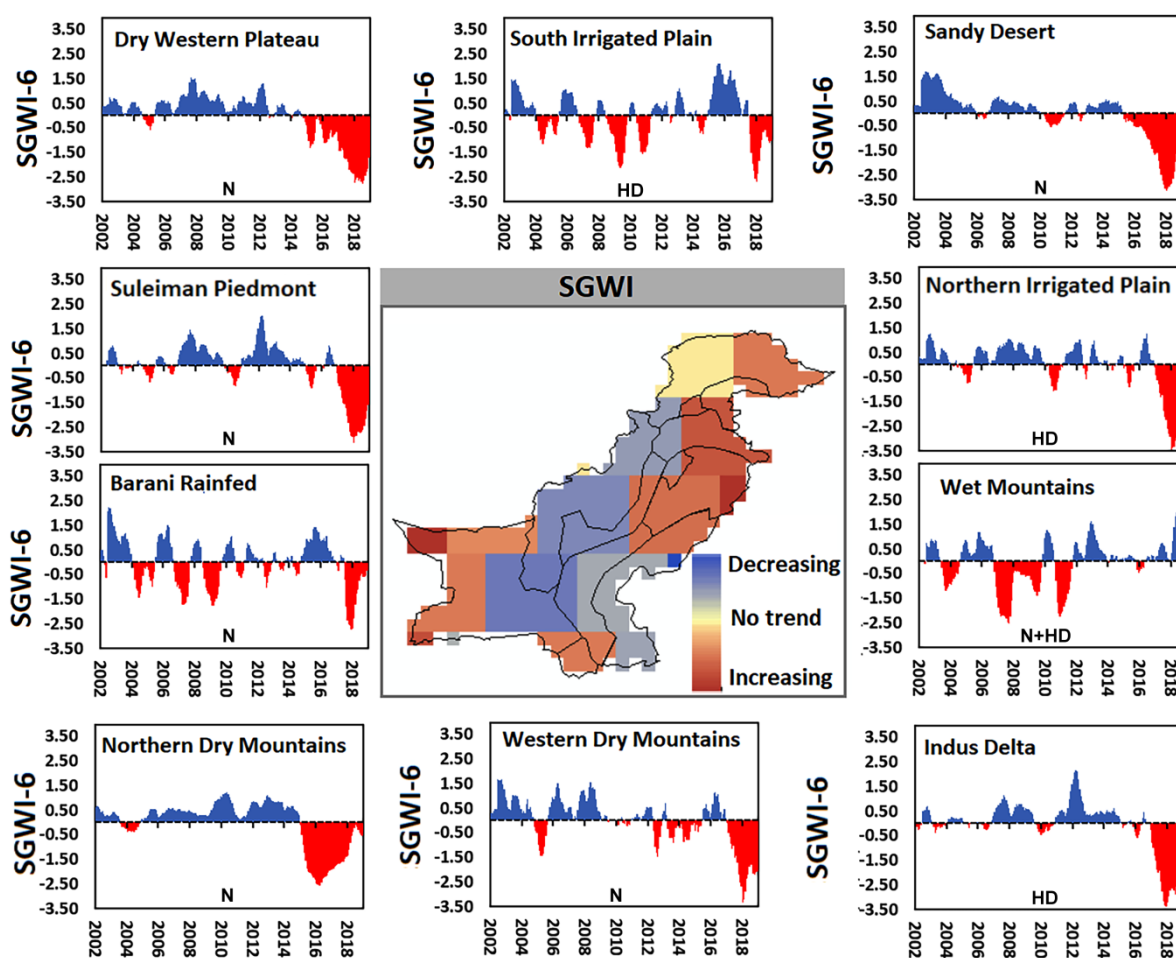


Figure 5. Spatial trend and time series of standardized groundwater storage index at a 6-month timeframe (SGWI-6) for 10 different AEZs. Note: N and HD represent natural and human-disturb zones, respectively.

Overall, the spatial pattern (trend) of hydro-meteorological droughts reflected by each indicator is different across the AEZs; however, an increasing trend is observed in downstream human-disturbed zones (e.g., SIP) based on SPEI, SSWSI, and SSFI, but not based on SGWI, which suggests a decreasing trend in groundwater drought; this may be associated with the fact that irrigation primarily relies on surface water, as shown in Figure 1c. The interannual rainfall variability and extreme high temperatures have made the downstream zones more vulnerable to drought risks [17,33], which may be explained by the concomitant lower precipitation and discharge resulting in hydrological drought [92]. Notably, one-third of the global population lives in water-scarce regions, particularly over

arid to semi-arid regions of Asia, the Middle East, North Africa, and the Mediterranean countries [93], where anthropogenic activities largely influence the groundwater resources [94]. We also evaluated the seasonal distribution of hydro-meteorological conditions for SPEI, SSWSI, SSFI, and SGWI in two main cropping seasons, namely, Rabi (corresponding to winter crops) and Kharif (corresponding to summer crops). It was seen that the drought years explained by hydro-meteorological indices were more frequent and intense during the Rabi season compared to Kharif (see Figure S3 in the Supplementary Material). These findings are in good agreement with previous studies across SA [81].

3.2. Evaluation of Drought Characteristics

We statistically evaluated attributes of hydro-meteorological drought propagation characteristics based on duration, frequency, months, and intensity in natural (N) and human-disturbed (HD) AEZs (Figure 6). Average drought intensity for each drought indicator, except SSFI, was higher in the human-disturbed zones than the natural zones. The maximum drought intensity was recorded as -2.8 for SGWI, followed by -2.2 for SSWSI and -1.7 for SSFI. The drought intensity in recent years is a sign that rainfall following droughts was insufficient to restore the hydrological conditions to fulfill the growing demand for agricultural, urban, and industrial sectors [95]. The number of drought months was higher for meteorological droughts (SPEI) than hydrological droughts (reflected by SSWSI, SGWI, and SSFI) across all natural zones. For example, the maximum drought months calculated with SPEI was 90 in zone 5 (Suleman Piedmont), whereas the maximum drought months for the SSWSI and SGWI in the same zone were 30 and 23 months, respectively. Drought duration calculated based on all hydro-metrological indicators had no significant difference in natural and human-disturbed AEZs. According to SPEI, the maximum drought termination duration was recorded as 9.25 months across the natural zone (Western Dry Mountains; WDM), which can be linked to the region's dry climate and lower precipitation rate [33]. However, based on SSFI, SSWSI, and SGWI, drought termination durations were significantly longer across the human-disturbed zone (North Irrigated Plain; NIP), reaching 16, 19, and 25 months, respectively (Table 2). Overall, drought termination durations frequently last longer with a slower termination rate than across human-disturbed zones subject to different anthropogenic activities, including water use for urbanization and agriculture and mixed influences [37,39]. In contrast, the drought termination rate appears to be higher in natural zones (with water transfer characteristics), measuring 0.86 mm/month for Northern Dry Mountains (NDM), 0.72 mm/month for Western Dry Mountains (WDM), and 0.61 mm/month for Indus Delta (ID). Because the termination rate is calculated from the termination duration (DT_{dur}) and maximum intensity (MI), any change in termination rate can result from either DT_{dur} or MI in a system [57]. Most natural regions had relatively short drought termination durations and fast drought termination rates. However, in some areas with anthropogenic operations, the termination rate is lower, but the system returned from drought to non-drought conditions in a shorter time period [57,59,96]. For instance, the mean termination durations and the corresponding rates calculated by SSWSI were 14.25 months (0.28 mm/month) and 3.86 months (0.28 mm/month) for SD (Sandy Desert) and ID (Indus Delta), respectively.

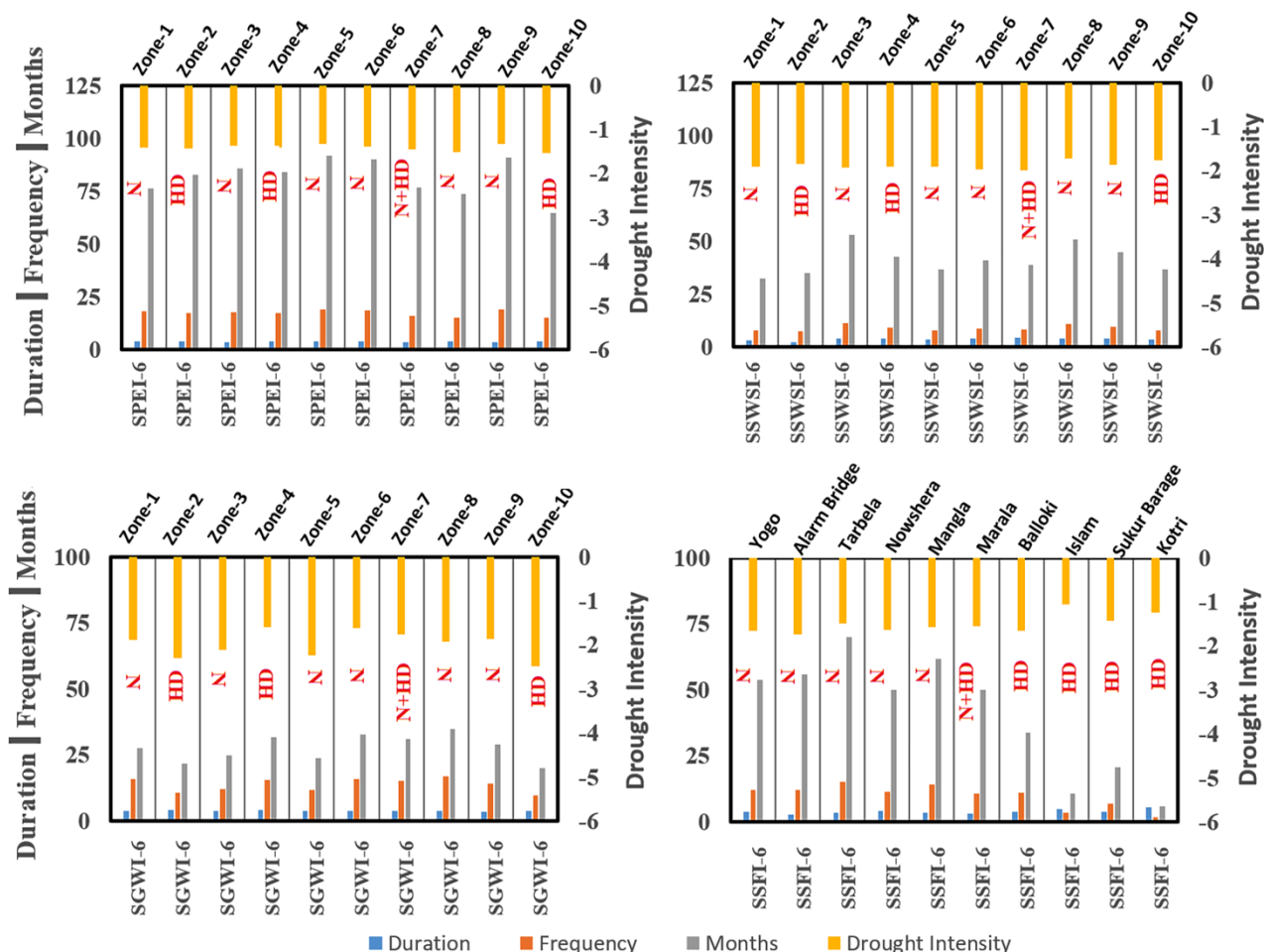


Figure 6. Distribution of hydro-meteorological drought events (duration, intensity, drought months, and frequency) for SPEI, SWSI, SGWI and SSFI, in natural (N) and human-disturbed (HD) AEZs. (Note: SPEI, TWSI, and SGWI were computed over 10 different AEZs, whereas SSFI was derived for 10 stream gauging stations distributed in different zones).

Table 2. Drought termination characteristics in different zones.

Zone	Condition	Mean Termination Duration (Month)				Mean Termination Rate (mm/Month)			
		SPEI	SSFI	SSWSI	SGWI	SPEI	SSFI	SSWSI	SGWI
DWP	Natural	5.88	**	6.50	5.00	0.65	**	0.41	0.55
SIP	Human-disturbed	4.71	14.33	4.20	11.00	0.59	0.20	0.29	0.25
SD	Natural	6.11	23.50	14.25	10.00	0.20	0.18	0.28	0.28
NIP	Human-disturbed	5.28	16.00	19.00	25.80	0.42	0.13	0.11	0.10
SPD	Natural	4.42	**	3.17	9.00	0.63	**	0.54	0.23
BRR	Natural	8.22	11.60	12.75	6.80	0.28	0.23	0.21	0.33
WM	Natural + Human-disturbed	4.70	6.07	28.00	9.66	0.56	0.34	0.13	0.24
NDM	Natural	7.16	5.62	11.75	13.00	0.86	0.30	0.11	0.21
WDM	Natural	9.25	**	2.22	6.33	0.38	**	0.72	0.36
ID	Human-disturbed	4.98	12.31	3.86	12.00	0.61	0.31	0.50	0.28

DWP—Dry Western Plateau; SIP—South Irrigated Plain; SD—Sandy Desert; NIP—Northern Irrigated Plain; SPD—Suleiman Piedmont; BRR—Barani-Rainfed; WM—Wet Mountains; NDM—Northern Dry Mountains; WDM—Western Dry Mountains; ID—Indus Delta. ** Data is not available for these regions.

3.3. Large-Scale Circulation Patterns and Composite Drought Events

The composites of large-scale circulation patterns associated with historical droughts were investigated over Pakistan (Figure 7). The composite drought years identified by various hydro-meteorological indicators were 1981–1983, 1999–2004, and 2018 (Figure 7a). These drought years were grouped together and further analyzed as a single variable. This method has been widely used to reveal the dominant patterns of large scale climate variables for drought assessment [47]. Composites of 500 hPa geopotential height anomalies depict a high-pressure system over Pakistan. Furthermore, the two-meter air temperature and soil temperature reveal positive anomalies, indicating hotter and drier climate favoring droughts in the region. As expected, the opposite patterns are apparent in the composites of 850 mb relative humidity, total precipitation, and soil moisture anomalies (Figure 7b). The year 1997–1998 was marked by a strong El Niño Southern Oscillation (ENSO). This strong ENSO induced the historically worst drought (1999–2002) in south-west Asia [30], affecting about 3.3 million people in Pakistan, and severely reducing the agricultural productivity [18].

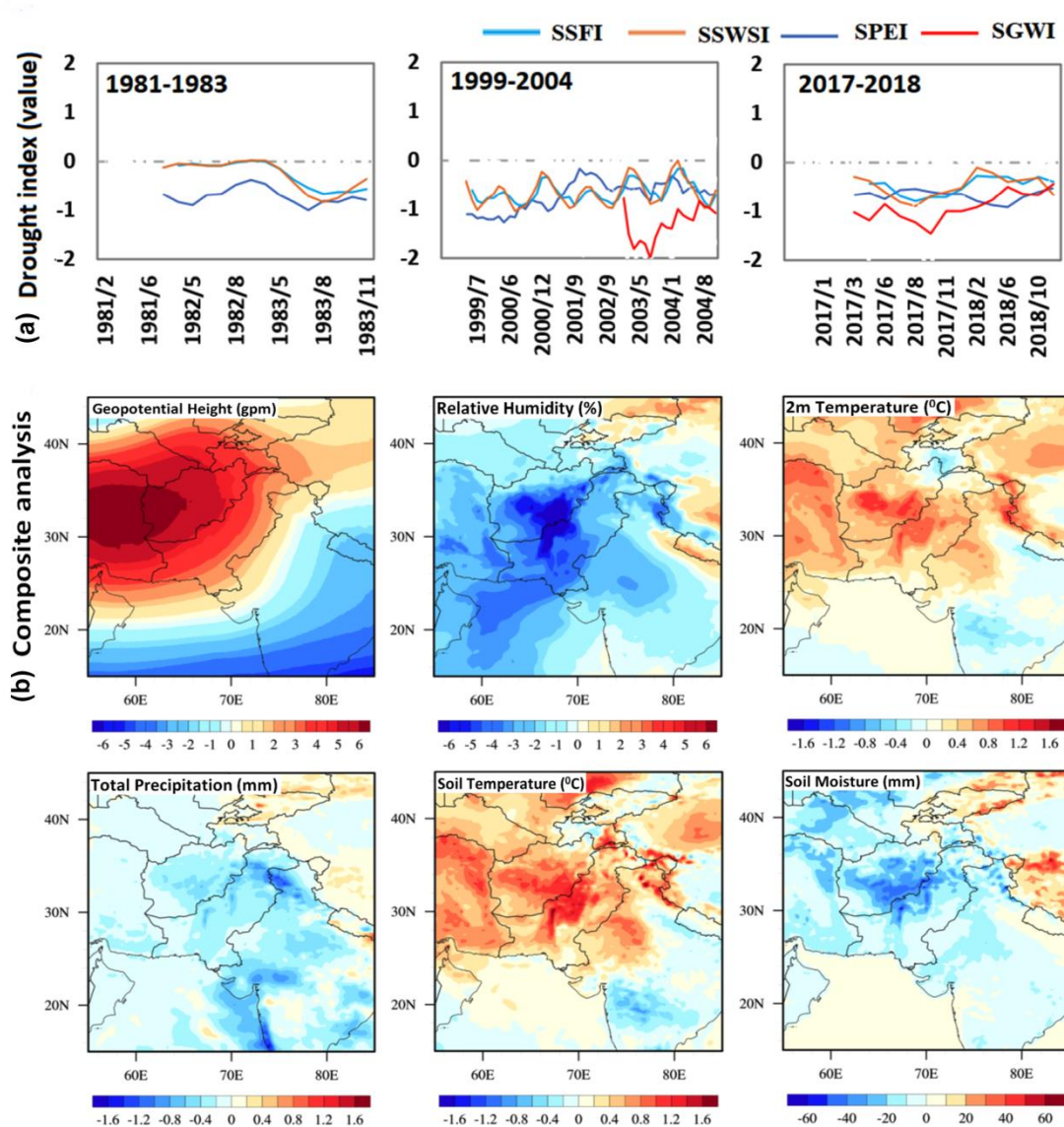


Figure 7. Composite drought years (a) and composite anomalies (b) of the large-scale circulation patterns (i.e., 500 hPa geopotential height, 850 mb relative humidity, 2 m temperature, total precipitation, soil temperature, and soil moisture) during historical (1981–1983, 1999–2004, 2017–2018) drought episodes.

3.4. Historical Variations in Agricultural-Based DSI and Crop Yield

The negative values of DSI represent moderate to severe (yellow to red color bar) drought conditions, and the positive values indicate normal to wet conditions (green to blue color bar) for vegetation growth (Figure 8). The spatial patterns of DSI reveal a drying pattern in the region during the years 2000, 2001, 2002, and 2004. The negative values of DSI show vegetation stress conditions for the zones of Indus Delta, Southern Irrigated Plain, Sandy Desert, Northern Irrigated Plain, Dry Western Plateau, and Suleiman Piedmont. In contrast, few AEZs depicted positive (higher) DSI values even during the drought years; this is mainly attributed to water resource availability, which tends to alleviate the moisture stress for crops [92]. Further, the regional average time-series analysis of standardized NDVI indicates a decline in vegetation growth during the intense drought episodes (Figure 8). ENSO-induced changes to vegetation stress conditions are already evident in the literature [97,98].

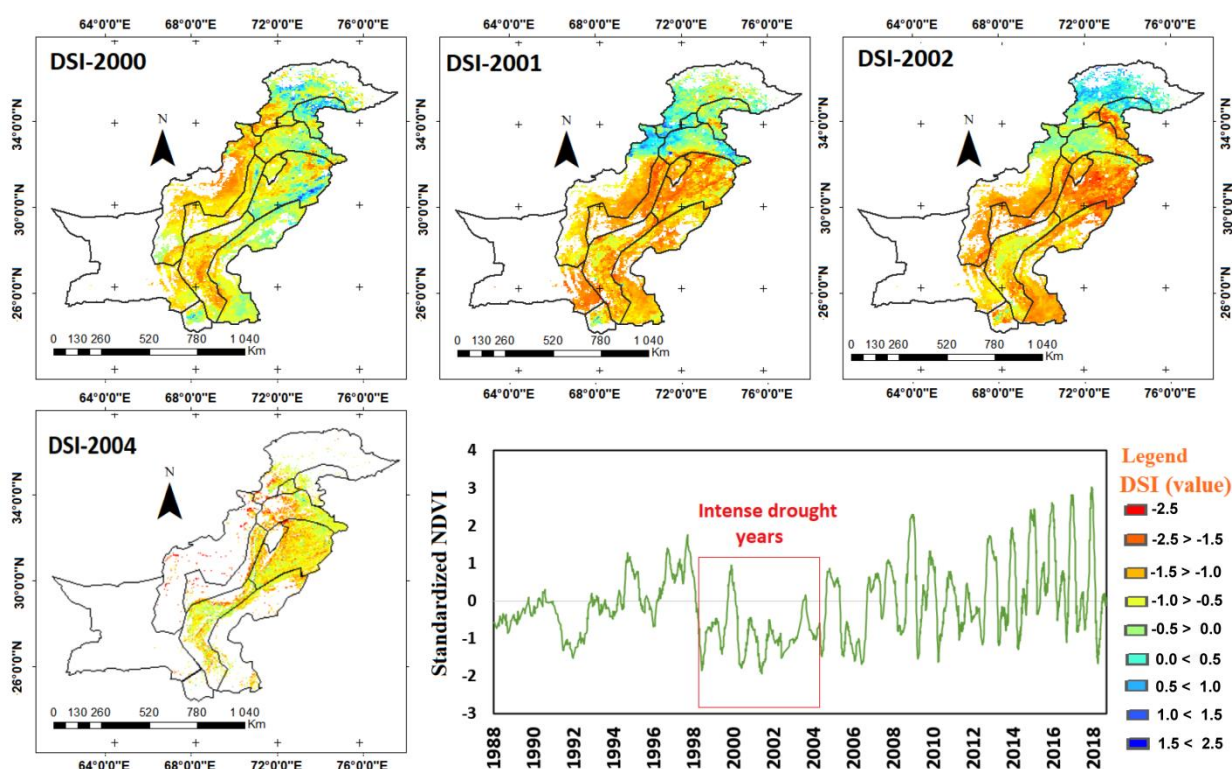


Figure 8. Spatial variations in Landsat drought severity index (DSI) in dry years (2000–2004) and average time series of NDVI from 1987–2018. Maps were prepared from Landsat images.

Figure 9a shows the rate of change in crop yield of five major crops over 123 locations in 1981–2017. It is observed that crop yield changes are not homogeneous throughout the study region. For instance, wheat yield decreased by 5–10 ton/ha/year in Western Dry Mountains and Dry Western Plateau, whereas it increased 5–11 ton/ha/year in Northern Irrigated Plain. On average, the greatest decrease in crop production was found for wheat and maize crops. Further, a non-parametric Mann–Kendall (MK) test was used to investigate the significance of long-term (1981–2017) trends in crop yield changes in different AEZs of Pakistan (see Table S2 in the Supplementary file). On average, the linear trend of the wheat, rice, and maize over most of the AEZs showed a significant increase in yield from 1981 to 2017. However, the trends seem to significantly decrease for some crops, such as sugarcane (in the Northern Dry Mountains), maize (in the Southern Irrigated Plain), rice (in the Wet Mountains), and cotton (in the Indus Delta) (see Table S2 in the Supplementary file). In Bangladesh, droughts have affected 1.2 million ha of rice fields during the growing season of Rabi and Kharif [99]. The dry spells for the 2008/09 winter season

impacted 70% of the agricultural areas in Nepal [100], whereas prolonged drought episodes from 2002 to 2012 caused widespread damage to food crops in India [81]. Changes in yield over time are influenced by various factors in addition to climate conditions, including new management methods, innovations, and crop planting area, resulting in a rising trend in yield [76]. Therefore, we detrended the historical crop yield to exclude the influence of these non-climatic shifts and thus isolate the variation caused by climate. Figure 9b shows the time-series variations in the standardized yield residuals index (SYRI) for five major crops over different AEZs in the study area from 1981 to 2017. SYRI of the maize, wheat, and cotton crops showed that yield increased from 1981 to 1993 and from 2006 to 2015. However, frequent yield loss was observed during drought episodes between 1998 to 2005 due to an intense El Niño event [18,33]. For instance, extreme yield loss ($SYRS \leq -1.5$) years were recorded for wheat (1981, 2001), cotton (1983, 1993, 2016), sugarcane (1986, 1989, 2005), maize (2000, 2003, 2005), and rice (1993, 2000), which are associated with drought episodes. Overall, the number of low-yield years ($SYRI \leq -1.5$) was greater for sugarcane and maize (10 years) followed by rice (9), wheat (8), and cotton (6).

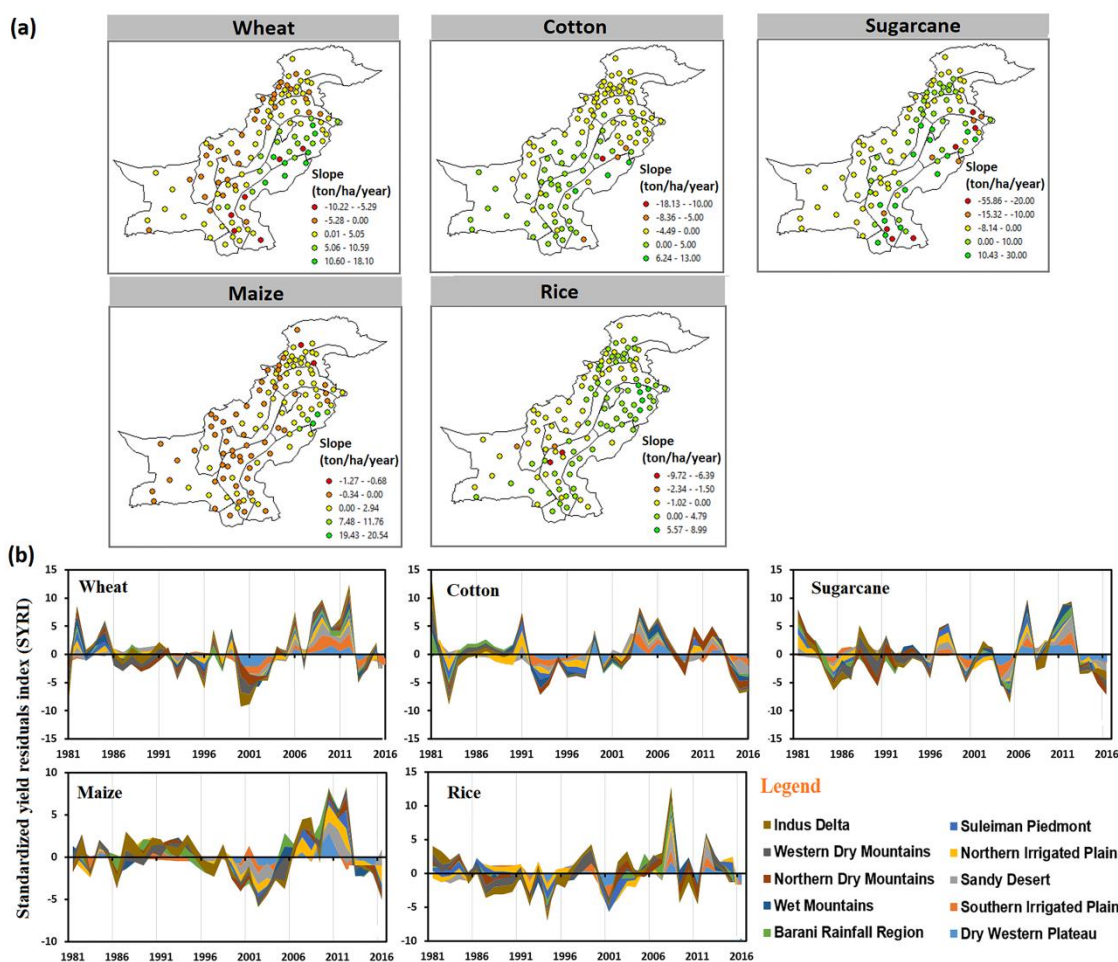


Figure 9. (a) The rate of change in crop yield for five major crops over 123 locations, and (b) comparison between standardized crop yield residual index (SYRI) for five major crops from 1981 to 2017 over different AEZs.

3.5. Accounting for Crop Yield Sensitivity and Losses

Drought effects on different crop growth stages (sowing, growth, and harvesting) were studied using monthly Pearson correlation coefficients between SYRI for five crops and hydro-meteorological indicators from 1981 to 2017 (Figure 10a–e). The positive values of correlation depicted the significant impact of drought indicators on crop yields. The

correlation values (minimum to maximum) indicated by box plots vary among each drought indicator and among growth stages. During the sowing to growth stages, the strongest correlation was observed primarily for wheat, sugarcane, and maize. For example, the correlation coefficient for winter wheat from sowing to harvesting ranges from $r = -0.60$ to 0.59 ($p \leq 0.05$), with the highest correlation observed during the sowing and the growth (third leaf's appearance from October–November) stages. In contrary, the maximum correlation through all drought indicators was higher during the growth and harvesting stage for maize. Overall, the correlation values appear to be higher using SGWI for all crops. Zone-wise, the analysis depicted that there is strong heterogeneity in correlation among all AEZs (Figure 10f–j). Overall, the maximum correlation was recorded over the Dry Western Plateau (DWP), South Irrigated Plain (SIP), Northern Dry Mountains (NDM), and Western Dry Mountains (WDM), indicating that that droughts in these regions had significant effects on crop production [101], which may be attributed to the fact that drought termination durations are frequently longer with the slower termination rate, as reported in Table 2. However, correlation values for each crop vary among AEZs. For instance, maximum values of correlation for rice were recorded in the Western Dry Mountains (WDM), and Indus Delta (ID), whereas the lowest values were recorded in the Dry Western Plateau (DWP) (Figure 10f–j).

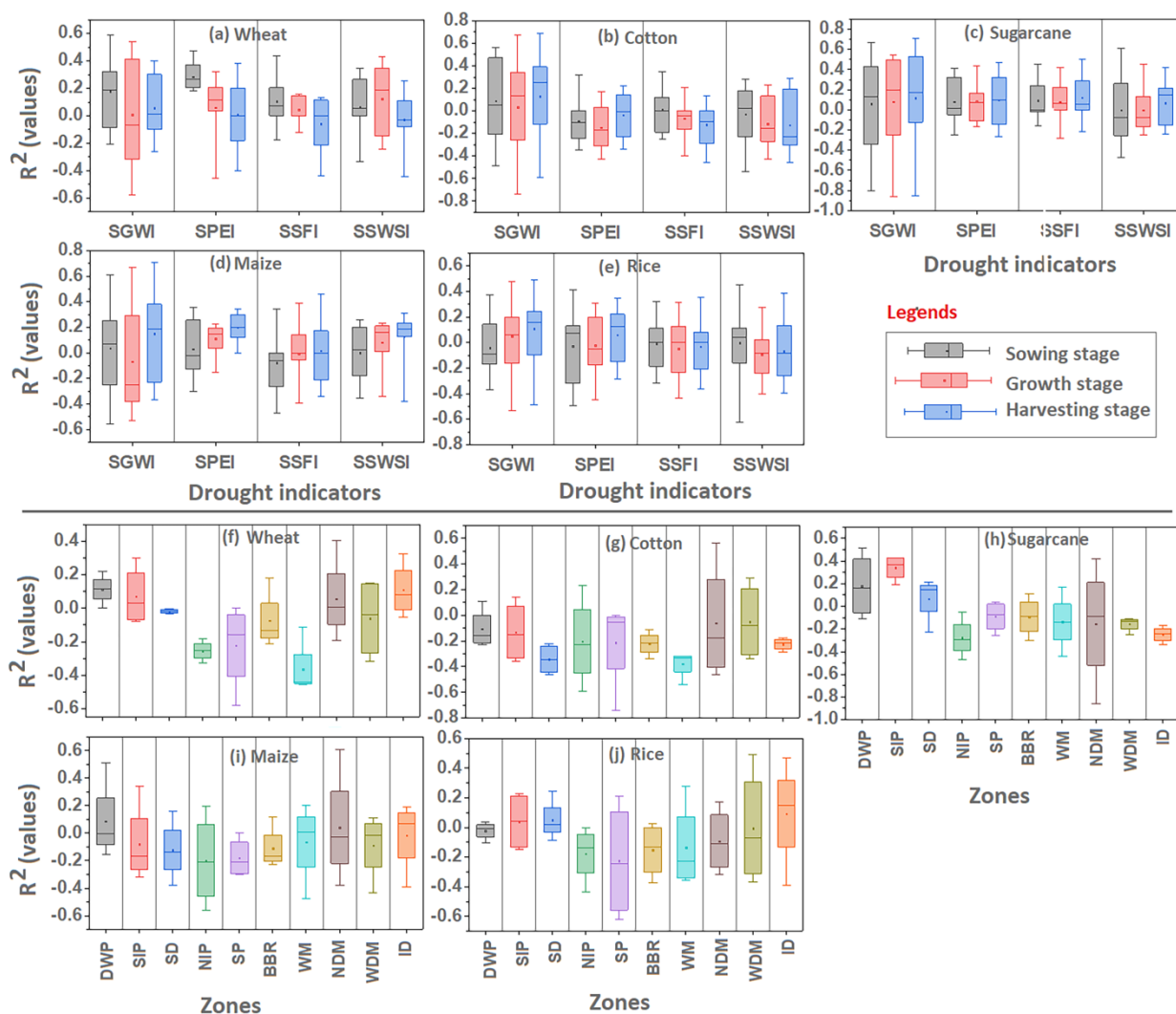


Figure 10. (a–e) Box plot (minimum–maximum) values of the correlation coefficient between drought indicators and SYRI in different crop growth stages, and (f–j) average correlation between SYRI and combined drought indicators across different AEZs from 1981–2017.

Figure 11a shows the time-averaged sensitivity of total crop production in response to changes in hydrological indicators (precipitation, surface water storage (SWS), groundwater storage (GWS), and streamflow) across the natural and human-disturbed AEZs. It is observed that yield sensitivity of total crop production tends to be higher with SWS, GWS, and streamflow variations in human-disturbed zones, except for precipitation variations, which are more sensitive in natural zones. The higher sensitivity of crop yield in human-disturbed zones is associated with the frequently longer termination duration and the slower termination rate of these indicators (Table 2). Figure 11b shows the time-series variations in area-averaged crop yield sensitivity of each crop in response to precipitation, SWS, and streamflow variations from 1981 to 2017. For instance, the higher peaks of extreme yield-sensitive years were observed during drought years, as found for wheat (2003, 2004, 2005), cotton (1993, 2000, 2001, 2016), sugarcane (1996, 2003, 2005), maize (1996, 2003), and rice (1988, 1993, 2003). Rice production seems to be more affected than other crops, with a maximum yield sensitivity value recorded as 9, followed by sugarcane (6.5), maize (6), wheat (5), and cotton (5).

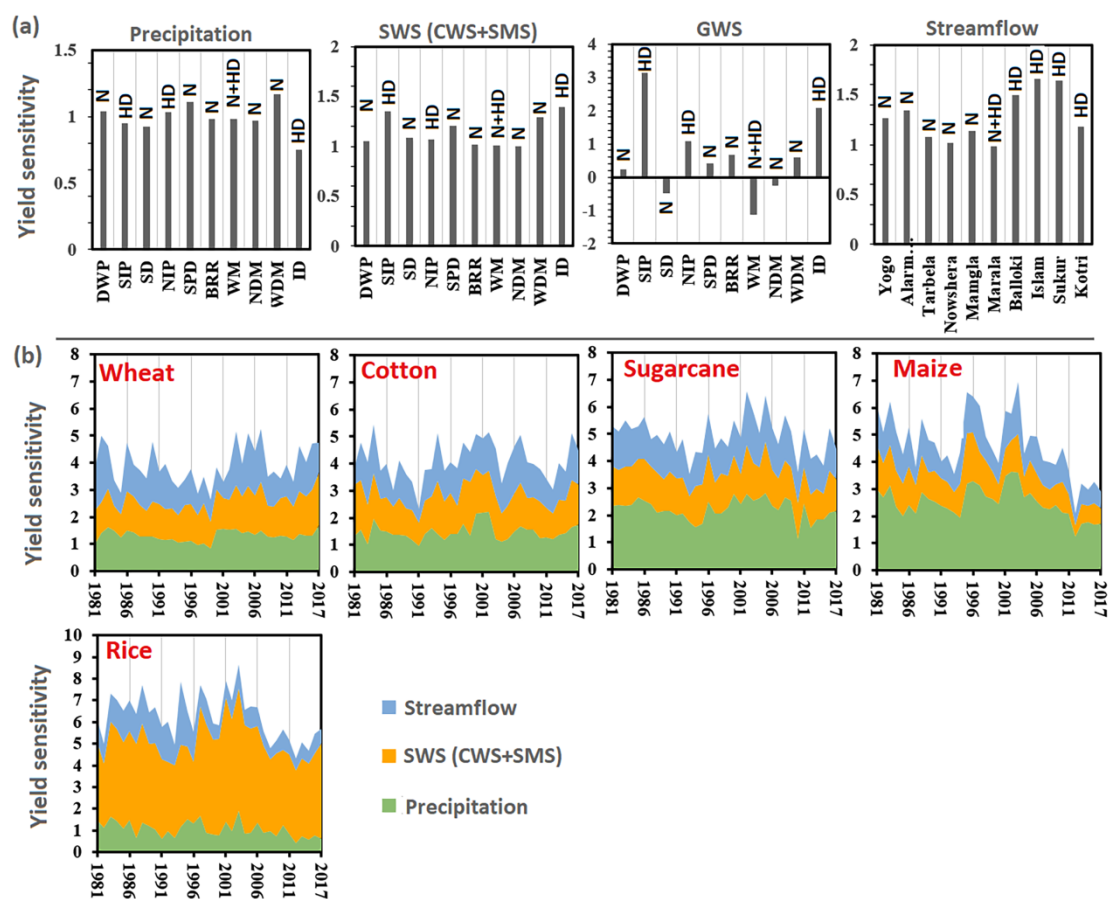


Figure 11. (a) Time-averaged sensitivity of total crop production in response to precipitation, surface water storage (SWS), groundwater storage (GWS), and streamflow changes from 1981 to 2017 over different AEZs, and (b) area-averaged crop yield sensitivity of each crop in response to precipitation, SWS, and streamflow changes from 1981 to 2017.

Table 3 shows that the percentage yield losses for five major crops during 1981–2017. The maize crop was most affected by droughts, with yields falling by 51% in 1985, followed by cotton at 45% in 2010 and rice at 37% in 2001, whereas wheat yields were less affected (Table 3). The crop yield losses differ depending on which hydro-meteorological predictor (SPEI, SSWSI, SSFI, and SGWI) is used (Table 3), and also depend on the crop-specific water requirement [35,36]. The percentage yield losses associated with shifts in

SSFI and SWSI were greater than in SPEI due to the longer termination time and slower termination rate for all crops. For instance, the maximum maize yield losses were 52% and 32% with SSFI and SWSI, respectively, and 28% with SPEI. The arid to semi-arid zones are more vulnerable to drought risk because of the interannual rainfall variability and the extensive use of surface water and sub-surface water resources [18,37].

Table 3. Quantification of crop yield losses (%) during intense drought episodes from 1981 to 2017.

Year	Wheat				Cotton				Sugarcane				Maize				Rice			
	SPEI	SSWSI	SSFI	SGWI	SPEI	SSWSI	SSFI	SGWI	SPEI	SSWSI	SSFI	SGWI	SPEI	SSWSI	SSFI	SGWI	SPEI	SSWSI	SSFI	SGWI
1982	0	19	0	0	0	0	0	0	0	15	11	0	0	0	29	0	0	0	23	0
1983	0	13	0	0	0	38	13	0	0	15	0	0	27	15	0	0	16	0	0	0
1984	19	0	12	0	0	19	0	0	16	0	15	0	0	39	0	0	0	20	0	
1985	0	0	16	0	0	0	0	0	0	0	20	0	5	11	51	0	8	0	36	0
1987	0	12	0	0	23	0	0	0	0	0	0	0	25	0	0	0	15	0	0	0
1988	13	0	0	0	8	23	13	0	19	0	0	0	0	0	0	0	6	0	0	0
1989	0	0	12	0	14	19	0	0	0	0	15	0	26	17	27	0	15	0	13	0
1992	0	14	0	0	0	28	14	0	0	16	0	0	0	0	0	0	0	0	0	0
1993	0	0	0	0	30	0	0	0	0	0	13	0	0	0	44	0	0	0	22	0
1994	0	0	0	0	0	0	16	0	0	30	0	0	0	0	0	0	0	0	0	0
1999	15	0	0	0	0	0	0	0	14	0	0	0	0	0	0	0	0	8	0	0
2000	23	0	0	0	19	29	0	0	23	0	14	0	19	0	0	0	15	23	0	0
2001	16	0	15	0	21	34	0	0	0	0	26	0	21	17	2	0	19	37	9	0
2002	18	0	0	0	15	0	0	0	0	0	17	0	0	0	0	0	17	21	0	0
2004	20	0	0	0	0	0	0	0	0	0	14	0	0	32	28	19	0	0	24	17
2005	0	16	0	13	0	0	0	0	0	12	0	16	0	0	0	0	0	0	0	0
2006	12	0	0	0	0	0	0	12	0	12	0	11	0	0	0	0	0	0	0	0
2007	0	19	0	0	0	0	0	14	0	13	0	14	0	0	0	0	0	0	0	0
2011	15	0	0	0	0	45	15	23	0	0	0	0	0	0	0	0	0	0	0	0
2015	0	14	0	0	0	35	12	16	0	17	0	16	0	0	0	15	0	0	0	0
2016	0	11	9	0	0	21	0	0	18	10	0	0	28	0	0	17	19	0	0	0

4. Discussion

The study area covers AEZs that have diverse topography with varying hydro-climate constraints [29]. Therefore, characterizing drought conditions based on a single constraint can produce an incomplete or even misleading picture. The present study evaluated the impacts of droughts on crop production by considering various hydro-meteorological and agricultural droughts indicators, such as SPEI, SSFI, SWSI, SGWI, and DSI. Spatiotemporal patterns of SPEI indicated extreme drought conditions in Southern Pakistan. A recent study investigated moderate to severe drought episodes in the arid region of Baluchistan, Pakistan, suggesting that the meteorological-based SPEI index adequately captures dry events in contrast to SPI, which does not take into account temperature, a critical factor for drought characterization [102]. Various previous studies further confirmed the use of SPEI for meteorological drought analysis over SA [32,46,48,79,80]. Notably, arid to semi-arid AEZs (i.e., Western Dry Mountains, Dry Western Plateau) experienced more frequent drought episodes, indicating their vulnerability to climate threats [18,82]. The extreme high-temperature events and below-average rainfall are critical factors of meteorological droughts in semi-arid environments [81]. Hydroclimate variability over the SA domain has been significantly influenced by ENSO episodes, particularly between 1998 and 2003 [33]. Notably, historical drought events have badly affected the socioeconomic and environmental conditions across the globe [79,99,103].

SSFI time series for stream gauge stations located in the natural zones (Wet Mountains and Northern Dry Mountains zones) experienced less frequent droughts [92]. Due to less anthropogenic influences, the streamflow data from these stations represent the natural condition, and changes in streamflow are mainly attributed to climate variability. Water transfer catchments with natural streamflow have fewer severe and extreme droughts than human-impacted systems [57]. By comparison, streamflow stations located

in the human-disturbed regions display more frequent drought conditions. Previous studies also found that rising food demands and climate threats, along with population growth, have greatly increased the risk of water shortage in Pakistan's irrigated regions [36,104].

SSWSI is also influential in driving the surface water storage cycle, and it is a key indicator in the evaluation of drought based on extreme hydrological events [105]. More frequent hydrological droughts based on SSWSI were recorded at Barani-Rainfed and Western Dry Mountains, which may be related to the extensive use of groundwater resources during dry season irrigation, and to climate variability [106,107]. Earlier studies further confirmed the impacts of water abstraction on hydrological droughts worldwide [86,87]. The interannual rainfall variability and extreme high temperatures have also made these zones more vulnerable to drought risks [17,33]. The long-term changes in the surface water storage are negatively correlated with ENSO. Simultaneously, the modulation of Pacific Decadal Oscillation (PDO) may significantly impact this relation [108].

Groundwater storage based on SGWI depicted that the human-disturbed zones (Northern Irrigated zone) are threatened by extensive groundwater depletion, forcing the region into persistent groundwater drought [50,109]. In addition, the southwestern region shows a significant decline in groundwater levels due to continuous groundwater storage depletion in recent decades [37]. The sensitivity of groundwater storage to hydroclimate constraints is evident in the literature; however, anthropogenic activities had a more significant effect on groundwater recharge than climate change [88,90,91]. The effects of hydro-metrological indicators are not the same throughout the study region, affecting the drought termination characteristics (termination duration and rate) across the natural and human-disturbed AEZs. For example, the ID plain shows a quicker transition from its most intense month of drought back to non-drought conditions compared to SD. This may be linked to the region's active water management practices, such as water-saving through adapting cropping patterns to the current irrigation settings, and even the combined implementation of optimal cropping patterns and improved irrigation technologies, i.e., sprinkler and drip irrigation [36]. Human-disturbed systems appear to increase the average drought termination duration and the rate at which the system returns from the peak of drought to non-drought conditions [57].

The spatial and temporal patterns of DSI depict vegetation stress conditions in the human-disturbed AEZs. Vegetation changes during intense dry spells have been linked to different ENSO phases [97,98]. However, fewer AEZs revealed positive (higher) DSI values during the dry years, mainly due to water resource availability, which alleviates crop moisture stress [92]. Overall, the analysis of hydrometeorological and agricultural drought indices showed different frequency and intensity of drought events across AEZs, which are subject to varying climate and land-use constraints. The AEZs having naturalized climate conditions register less frequent drought events. These naturalized AEZs are mostly located over the core monsoon region of Pakistan, which receive rainfall during the summer season and winter rainfall in the form of snow [83], and have relatively short drought termination durations and fast drought termination characteristics [57,59,96]. In addition to climate variability, the catchment characteristics (i.e., geology, area, and lag-time) also play an important role in drought propagation. Human-disturbed AEZs experience the most frequent drought events, suggesting that human activities are more inclined to play a negative role in aggravating droughts by altering the flow regime and their spatiotemporal characteristics [86,87,90,91,110]. For instance, all AEZs except Barani-Rainfed and Wet Mountains show a continuous decline in groundwater storage and a shift from wetter to drier conditions during 2002–2018, which is probably associated with a large abstraction of groundwater for irrigation purposes [35,37]. The risks of climate change for crop production in Pakistan have been reported in the literature [101]. The composite analysis of atmospheric circulation revealed large-scale changes in geopotential height, near-surface air temperature, soil moisture conditions, relative humidity, and total precipitation are the likely drivers of droughts over Pakistan. The impacts of climate

change on agricultural productivity (i.e., rice, wheat, maize, cotton, and sugarcane) varied across AEZs due to different climate and hydrological constraints. Temperature is a dominant factor in defining drought episodes during the Rabi season, whereas rainfall influences the Kharif growing season [49]. Notably, an increase in the mean seasonal temperature above 25.5 °C severely impacts the wheat yield in arid and semi-arid environments [111]. Extreme high temperature has negatively impacted the maize crop yield in the Northern Dry Mountains zone [112]. The below-average rainfall amount also negatively influenced the yield of major food crops, especially in the rainfed regions [101].

Results from the current study suggest that sowing to growth stages are the most susceptible times in terms of water deficit for crop production, resulting in substantial yield loss [75]. Temperature variability is critical during crop development stages [33,36,37,101,113]. Robust increases in mean temperatures resulted in crop yield failure, causing damage to spikes or smaller grains at later crop development stages [111,112,114]. Global warming is expected to increase the risk of warmer temperatures that will likely impact crop plants [22]. The development of drought-tolerant high-yield varieties is needed to alleviate climate change impacts [101]. All the zones depict drought episodes in different periods; however, drought episodes from 2000–2004 occurred in most AEZs, affecting the yield (80%) of agricultural crops and GDP to a greater extent [41,42]. Wheat yield was impacted more in Northern Irrigated Plain, whereas the yields of rice and maize crops were largely impacted in the zones of the Western Dry Mountains [115]. Many other factors may also contribute to changes in crop production in the study area, including changes in population patterns, soil management technologies, the density and proportion of agricultural land, fertilizer type and availability, and capital invested [76,116]. However, we primarily studied the sensitivity of crop productivity to precipitation, SWS, GWS, and streamflow variations. Large crop yield variations with a slight variation in the hydro-climate constraints shows high sensitivity [22,60,75]. Based on our yield sensitivity index analysis, rice production is generally more sensitive than other crops. The yield sensitivity of total crop production seems to be higher in human-disturbed zones corresponding to SWS, GWS, and streamflow variations, which is related to the frequently longer termination duration and their slower termination rate of hydro-meteorological droughts.

5. Limitations and Future Directions

Our study tried to evaluate the historical crop yield losses associated with hydro-meteorological and agricultural drought propagation over different AEZs in the study region; however, there are still some limitations which may be the subject of future investigations. Groundwater storage analysis was presented for a short-term period of 2002–2018 due to data limitations from ground observations and the limited coverage of GRACE. In-depth groundwater studies are required to investigate the groundwater changes behind the GRACE data period. Although we compared the GRACE-driven GWSA estimates with observational data, additional uncertainty analysis is required to validate the other satellites and reanalysis products used in current study. In addition, future efforts should account for the variety of each crop in the AEZs, water balance, irrigation efficiency, and water productivity to better understand the effects of extreme hydro-meteorological droughts on each crop in the study area. Given the sensitivity of agricultural systems to hydro-meteorological drought, future research should investigate the new phenotypes capable of surviving extreme temperatures and producing higher yields in Pakistan's diverse agro-ecological conditions. This study served as a first step to explore how the potential impacts of extreme hydro-meteorological droughts are affecting the agro-ecosystem of the study region; however, deeper insight into the socio-economic and future climate impacts should be investigated. Notwithstanding these issues, the findings of the current study represent an important asset to identify emerging issues in a wider context with a focus on its potential applications to other South Asian regions.

6. Conclusions

This study demonstrated the utility of hydro-meteorological indicators in early crop yield assessment for drought mitigation and water resources management across various AEZs in Pakistan. The spatiotemporal changes in extreme hydro-meteorological droughts and their influence on crop yield variability were investigated across natural and human-disturbed AEZs. All hydro-meteorological indicators effectively captured the common drought episodes (1981–1983, 1999–2004, and 2017–2018) during historical analysis from 1981 to 2019. Large-scale changes in geopotential height, near-surface air temperature, soil moisture conditions, and total precipitation are the likely drivers of droughts in the region. The satellite-based NDVI and DSI depict a decreasing vegetation growth trend during extreme drought years. The drought periods based on SWSI, SGWI, and SSFI were more frequent and intense in human-disturbed AEZs compared to natural settings. Drought termination durations were frequently longer, corresponding to shorter termination rates in the human-disturbed AEZs compared with the natural zones. Percentage yield losses of major crops were found to be greater and more sensitive to SSFI and SWSI variations than SPEI due to the longer drought termination duration and slower termination rate of these indices.

Supplementary Materials: The following supporting information can be downloaded at: <https://www.mdpi.com/article/10.3390/rs14092152/s1>, Figure S1: Cropping calendar for major crops in the study region; Figure S2: Comparison of GRACE-based GWSA and observational wells; Figure S3: a, b, c, and d represent the seasonal distribution of hydro-metrological conditions based on a 6-month timescale for SPEI, STWSI, SSFI, and SGWI over 10 different agro-ecological zones, and e, f, g, and h represent the average seasonal conditions of SPEI, STWSI, SSFI, and SGWI for all zones from 1980 to 2019. RB represents the Rabi season and KH represents the Kharif season; Table S1: A detailed description of the investigated AEZs in Pakistan; Table S2: Results of the Mann–Kendall (Z value) test for 5 main crops grown in 10 different AEZs during 1981–2017. References [117,118] are cited in the supplementary materials.

Author Contributions: Conceptualization, F.S. and A.A.; methodology, A.A.; software, A.A. and F.S.; validation, F.S. and A.A.; formal analysis, A.A., F.S. and A.D.; investigation, F.S.; resources, X.Z.; data curation, A.D.; writing—original draft preparation, F.S. and A.A.; writing—review and editing, A.M., T.K. and Q.B.P.; visualization, T. K., M.M.R. and K.M.; supervision, X.Z.; funding acquisition, X.Z. All authors have read and agreed to the published version of the manuscript.

Funding: This work was financially supported by the National Natural Science Foundation of China, grant number 41991282 and the CAS-TWAS Centre of Excellence for Climate and Environment Sciences.

Data Availability Statement: No new data were created in this study. The datasets used for the study and their sources are briefly discussed in materials and methods section.

Conflicts of Interest: The authors declare no conflict of interest.

References

1. Portela, M.M.; dos Santos, J.F.; Silva, A.T.; Benitez, J.B.; Frank, C.; Reichert, J.M. Drought analysis in southern Paraguay, Brazil and northern Argentina: Regionalization, occurrence rate and rainfall thresholds. *Hydrol. Res.* **2015**, *46*, 792–810.
2. Al-Kaisi, M.M.; Elmore, R.W.; Guzman, J.G.; Hanna, H.M.; Hart, C.E.; Helmers, M.J.; Hodgson, E.W.; Lenssen, A.W.; Mallarino, A.P.; Robertson, A.E. Drought impact on crop production and the soil environment: 2012 experiences from Iowa. *J. Soil Water Conserv.* **2013**, *68*, 19A–24A.
3. Wan, W.; Liu, Z.; Li, J.; Xu, J.; Wu, H.; Xu, Z. Spatiotemporal patterns of maize drought stress and their effects on biomass in the Northeast and North China Plain from 2000 to 2019. *Agric. For. Meteorol.* **2022**, *315*, 108821.
4. Zhang, A.; Zheng, C.; Wang, S.; Yao, Y. Analysis of streamflow variations in the Heihe River Basin, northwest China: Trends, abrupt changes, driving factors and ecological influences. *J. Hydrol. Reg. Stud.* **2015**, *3*, 106–124.
5. Zeng, Z.; Wu, W.; Ge, Q.; Li, Z.; Wang, X.; Zhou, Y.; Zhang, Z.; Li, Y.; Huang, H.; Liu, G. Legacy effects of spring phenology on vegetation growth under pre-season meteorological drought in the Northern Hemisphere. *Agric. For. Meteorol.* **2021**, *310*, 108630.
6. Van Dijk, A.I.; Beck, H.E.; Crosbie, R.S.; de Jeu, R.A.; Liu, Y.Y.; Podger, G.M.; Timbal, B.; Viney, N.R. The Millennium Drought in southeast Australia (2001–2009): Natural and human causes and implications for water resources, ecosystems, economy, and society. *Water Resour. Res.* **2013**, *49*, 1040–1057.

7. Ding, Y.; Hayes, M.J.; Widhalm, M. Measuring economic impacts of drought: A review and discussion. *Disaster Prev. Manag. Int. J.* **2011**, *20*, 434–446.
8. Nam, W.-H.; Choi, J.-Y.; Yoo, S.-H.; Jang, M.-W. A decision support system for agricultural drought management using risk assessment. *Paddy Water Environ.* **2012**, *10*, 197–207.
9. Wu, H.; Wilhite, D.A. An operational agricultural drought risk assessment model for Nebraska, USA. *Nat. Hazards* **2004**, *33*, 1–21.
10. Gocic, M.; Trajkovic, S. Drought characterisation based on water surplus variability index. *Water Resour. Manag.* **2014**, *28*, 3179–3191.
11. Duffy, P.B.; Brando, P.; Asner, G.P.; Field, C.B. Projections of future meteorological drought and wet periods in the Amazon. *Proc. Natl. Acad. Sci. USA* **2015**, *112*, 13172–13177.
12. Zhao, T.; Dai, A. The magnitude and causes of global drought changes in the twenty-first century under a low-moderate emissions scenario. *J. Clim.* **2015**, *28*, 4490–4512.
13. Hui-Mean, F.; Yusop, Z.; Yusof, F. Drought analysis and water resource availability using standardised precipitation evapotranspiration index. *Atmos. Res.* **2018**, *201*, 102–115.
14. Theron, S.; Archer, E.; Midgley, S.; Walker, S. Agricultural perspectives on the 2015–2018 western cape drought, South Africa: Characteristics and spatial variability in the core wheat growing regions. *Agric. For. Meteorol.* **2021**, *304*, 108405.
15. Xu, L.; Chen, N.; Yang, C.; Zhang, C.; Yu, H. A parametric multivariate drought index for drought monitoring and assessment under climate change. *Agric. For. Meteorol.* **2021**, *310*, 108657.
16. Pachauri, R.K.; Allen, M.R.; Barros, V.R.; Broome, J.; Cramer, W.; Christ, R.; Church, J.A.; Clarke, L.; Dahe, Q.; Dasgupta, P. *Climate Change 2014: Synthesis Report. Contribution of Working Groups I, II and III to the Fifth Assessment Report of the Intergovernmental Panel on Climate Change*; IPCC: Geneva, Switzerland, 2014.
17. Saleem, F.; Zeng, X.; Hina, S.; Omer, A. Regional changes in extreme temperature records over Pakistan and their relation to Pacific variability. *Atmos. Res.* **2021**, *250*, 105407.
18. Hina, S.; Saleem, F. Historical analysis (1981–2017) of drought severity and magnitude over a predominantly arid region of Pakistan. *Clim. Res.* **2019**, *78*, 189–204.
19. Dogan, S.; Berkday, A.; Singh, V.P. Comparison of multi-monthly rainfall-based drought severity indices, with application to semi-arid Konya closed basin, Turkey. *J. Hydrol.* **2012**, *470*, 255–268.
20. Lloyd-Hughes, B. A spatio-temporal structure-based approach to drought characterisation. *Int. J. Climatol.* **2012**, *32*, 406–418.
21. Yao, Y.; Fu, B.; Liu, Y.; Li, Y.; Wang, S.; Zhan, T.; Wang, Y.; Gao, D. Evaluation of ecosystem resilience to drought based on drought intensity and recovery time. *Agric. For. Meteorol.* **2022**, *314*, 108809.
22. Vogel, E.; Donat, M.G.; Alexander, L.V.; Meinshausen, M.; Ray, D.K.; Karoly, D.; Meinshausen, N.; Frieler, K. The effects of climate extremes on global agricultural yields. *Environ. Res. Lett.* **2019**, *14*, 054010.
23. Bastos, A.; Ciaia, P.; Friedlingstein, P.; Sitch, S.; Pongratz, J.; Fan, L.; Wigneron, J.; Weber, U.; Reichstein, M.; Fu, Z. Direct and seasonal legacy effects of the 2018 heat wave and drought on European ecosystem productivity. *Sci. Adv.* **2020**, *6*, eaba2724.
24. Yuan, X.; Wang, L.; Wu, P.; Ji, P.; Sheffield, J.; Zhang, M. Anthropogenic shift towards higher risk of flash drought over China. *Nat. Commun.* **2019**, *10*, 4661.
25. Breshears, D.D.; Cobb, N.S.; Rich, P.M.; Price, K.P.; Allen, C.D.; Balice, R.G.; Romme, W.H.; Kastens, J.H.; Floyd, M.L.; Belnap, J. Regional vegetation die-off in response to global-change-type drought. *Proc. Natl. Acad. Sci. USA* **2005**, *102*, 15144–15148.
26. Peng, S.; Huang, J.; Sheehy, J.E.; Laza, R.C.; Visperas, R.M.; Zhong, X.; Centeno, G.S.; Khush, G.S.; Cassman, K.G. Rice yields decline with higher night temperature from global warming. *Proc. Natl. Acad. Sci. USA* **2004**, *101*, 9971–9975.
27. Kharin, V.V.; Zwiers, F.W.; Zhang, X.; Hegerl, G.C. Changes in temperature and precipitation extremes in the IPCC ensemble of global coupled model simulations. *J. Clim.* **2007**, *20*, 1419–1444.
28. Zhang, Q.; Xu, C.-Y.; Zhang, Z.; Chen, Y.D. Changes of temperature extremes for 1960–2004 in Far-West China. *Stoch. Environ. Res. Risk Assess.* **2009**, *23*, 721–735.
29. Hanif, M.; Khan, A.H.; Adnan, S. Latitudinal precipitation characteristics and trends in Pakistan. *J. Hydrol.* **2013**, *492*, 266–272.
30. Barlow, M.; Zaitchik, B.; Paz, S.; Black, E.; Evans, J.; Hoell, A. A review of drought in the Middle East and southwest Asia. *J. Clim.* **2016**, *29*, 8547–8574.
31. Anjum, S.A.; Wang, L.; Salhab, J.; Khan, I.; Saleem, M. An assessment of drought extent and impacts in agriculture sector in Pakistan. *J. Food Agric. Environ.* **2010**, *8*, 1359–1363.
32. Ahmed, K.; Shahid, S.; Nawaz, N. Impacts of climate variability and change on seasonal drought characteristics of Pakistan. *Atmos. Res.* **2018**, *214*, 364–374.
33. Adnan, S.; Ullah, K.; Gao, S.; Khosa, A.H.; Wang, Z. Shifting of agro-climatic zones, their drought vulnerability, and precipitation and temperature trends in Pakistan. *Int. J. Climatol.* **2017**, *37*, 529–543.
34. Rasul, G.; Mahmood, A.; Sadiq, A.; Khan, S. Vulnerability of the Indus delta to climate change in Pakistan. *Pak. J. Meteorol.* **2012**, *8*, 89–107.
35. Hassan, G.; Hassan, F. Sustainable use of groundwater for irrigated agriculture: A case study of Punjab, Pakistan. *Eur. Water* **2017**, *57*, 475–480.
36. Muzammil, M.; Zahid, A.; Breuer, L. Water Resources Management Strategies for Irrigated Agriculture in the Indus Basin of Pakistan. *Water* **2020**, *12*, 1429.

37. Qureshi, A.S. Groundwater Governance in Pakistan: From Colossal Development to Neglected Management. *Water* **2020**, *12*, 3017.
38. Janjua, S.; Hassan, I.; Muhammad, S.; Ahmed, S.; Ahmed, A. Water management in Pakistan's Indus Basin: Challenges and opportunities. *Water Policy* **2021**, *23*, 1329–1343.
39. Qureshi, A.S. Improving food security and livelihood resilience through groundwater management in Pakistan. *Glob. Adv. Res. J. Agric. Sci.* **2015**, *4*, 687–710.
40. Ahmad, S.; Hussain, Z.; Qureshi, A.S.; Majeed, R.; Saleem, M. *Drought Mitigation in Pakistan: Current Status and Options for Future Strategies*; IWMI: Anand, India, 2004; Volume 85.
41. Rehman, A.; Jingdong, L.; Shahzad, B.; Chandio, A.A.; Hussain, I.; Nabi, G.; Iqbal, M.S. Economic perspectives of major field crops of Pakistan: An empirical study. *Pac. Sci. Rev. B Humanit. Soc. Sci.* **2015**, *1*, 145–158.
42. Sarwar, A. Droughts in Pakistan—a socio-political perspective. In *Droughts and Integrated Water Resource Management in South Asia: Issues, Alternatives and Futures*; SAGE Publications: New Delhi, India, 2008; pp. 200–230.
43. Xie, H.; Ringler, C.; Zhu, T.; Waqas, A. Droughts in Pakistan: A spatiotemporal variability analysis using the Standardized Precipitation Index. *Water Int.* **2013**, *38*, 620–631.
44. Adnan, S.; Ullah, K.; Gao, S. Characterization of drought and its assessment over Sindh, Pakistan during 1951–2010. *J. Meteorol. Res.* **2015**, *29*, 837–857.
45. Ullah, I.; Ma, X.; Yin, J.; Asfaw, T.G.; Azam, K.; Syed, S.; Liu, M.; Arshad, M.; Shahzaman, M. Evaluating the meteorological drought characteristics over Pakistan using in situ observations and reanalysis products. *Int. J. Climatol.* **2021**, *41*, 4437–4459.
46. Aadhar, S.; Mishra, V. High-resolution near real-time drought monitoring in South Asia. *Sci. Data* **2017**, *4*, 170145.
47. Hina, S.; Saleem, F.; Arshad, A.; Hina, A.; Ullah, I. Droughts over Pakistan: Possible cycles, precursors and associated mechanisms. *Geomat. Nat. Hazards Risk* **2021**, *12*, 1638–1668.
48. Shahzaman, M.; Zhu, W.; Ullah, I.; Mustafa, F.; Bilal, M.; Ishfaq, S.; Nisar, S.; Arshad, M.; Iqbal, R.; Aslam, R.W. Comparison of Multi-Year Reanalysis, Models, and Satellite Remote Sensing Products for Agricultural Drought Monitoring over South Asian Countries. *Remote Sens.* **2021**, *13*, 3294.
49. Ullah, I.; Ma, X.; Yin, J.; Saleem, F.; Syed, S.; Omer, A.; Habtemicheal, B.A.; Liu, M.; Arshad, M. Observed changes in seasonal drought characteristics and their possible potential drivers over Pakistan. *Int. J. Climatol.* **2022**, *42*, 1576–1596.
50. Iqbal, N.; Hossain, F.; Lee, H.; Akhter, G. Satellite gravimetric estimation of groundwater storage variations over Indus Basin in Pakistan. *IEEE J. Sel. Top. Appl. Earth Obs. Remote Sens.* **2016**, *9*, 3524–3534.
51. Salam, M.; Cheema, M.J.M.; Zhang, W.; Hussain, S.; Khan, A.; Bilal, M.; Arshad, A.; Ali, S.; Zaman, M.A. Groundwater storage change estimation using grace satellite data in Indus Basin. *Big Data Water Resour. Eng.* **2020**, *1*, 13–18.
52. Hussain, D.; Kao, H.-C.; Khan, A.A.; Lan, W.-H.; Imani, M.; Lee, C.-M.; Kuo, C.-Y. Spatial and Temporal Variations of Terrestrial Water Storage in Upper Indus Basin Using GRACE and Altimetry Data. *IEEE Access* **2020**, *8*, 65327–65339.
53. Dilawar, A.; Chen, B.; Arshad, A.; Guo, L.; Ehsan, M.I.; Hussain, Y.; Kayiranga, A.; Measho, S.; Zhang, H.; Wang, F. Towards Understanding Variability in Droughts in Response to Extreme Climate Conditions over the Different Agro-Ecological Zones of Pakistan. *Sustainability* **2021**, *13*, 6910.
54. Vicente-Serrano, S.M.; López-Moreno, J.I.; Beguería, S.; Lorenzo-Lacruz, J.; Azorin-Molina, C.; Morán-Tejeda, E. Accurate computation of a streamflow drought index. *J. Hydrol. Eng.* **2012**, *17*, 318–332.
55. Bloomfield, J.; Marchant, B. Analysis of groundwater drought building on the standardised precipitation index approach. *Hydrol. Earth Syst. Sci.* **2013**, *17*, 4769–4787.
56. Seo, J.Y.; Lee, S.-I. Spatio-temporal groundwater drought monitoring using multi-satellite data based on an artificial neural network. *Water* **2019**, *11*, 1953.
57. Margariti, J.; Rangelcroft, S.; Parry, S.; Wendt, D.; Van Loon, A.; Chadwick, O. Anthropogenic activities alter drought termination. *Elem. Sci. Anthr.* **2019**, *7*, 27.
58. Potopova, V.; Boroneanț, C.; Boincean, B.; Soukup, J. Impact of agricultural drought on main crop yields in the Republic of Moldova. *Int. J. Climatol.* **2016**, *36*, 2063–2082.
59. Parry, S.; Wilby, R.L.; Prudhomme, C.; Wood, P.J. A systematic assessment of drought termination in the United Kingdom. *Hydrol. Earth Syst. Sci.* **2016**, *20*, 4265–4281.
60. Khatiwada, K.R.; Pandey, V.P. Characterization of hydro-meteorological drought in Nepal Himalaya: A case of Karnali River basin. *Weather. Clim. Extrem.* **2019**, *26*, 100239.
61. Kim, D.-W.; Byun, H.-R.; Choi, K.-S.; Oh, S.-B. A spatiotemporal analysis of historical droughts in Korea. *J. Appl. Meteorol. Climatol.* **2011**, *50*, 1895–1912.
62. Ali, S.; Wang, Q.; Liu, D.; Fu, Q.; Rahaman, M.M.; Faiz, M.A.; Cheema, M.J.M. Estimation of spatio-temporal groundwater storage variations in the Lower Transboundary Indus Basin using GRACE satellite. *J. Hydrol.* **2022**, *605*, 127315.
63. Zhu, Y.; Liu, S.; Yi, Y.; Xie, F.; Grünwald, R.; Miao, W.; Wu, K.; Qi, M.; Gao, Y.; Singh, D. Overview of terrestrial water storage changes over the Indus River Basin based on GRACE/GRACE-FO solutions. *Sci. Total Environ.* **2021**, *799*, 149366.
64. Ali, S.; Liu, D.; Fu, Q.; Cheema, M.J.M.; Pham, Q.B.; Rahaman, M.; Dang, T.D.; Anh, D.T. Improving the Resolution of GRACE Data for Spatio-Temporal Groundwater Storage Assessment. *Remote Sens.* **2021**, *13*, 3513.
65. Chen, J.; Famiglietti, J.S.; Scanlon, B.R.; Rodell, M. Groundwater storage changes: Present status from GRACE observations. *Surv. Geophys.* **2016**, *37*, 397–417.

66. Bennett, G.D. *Analysis of Aquifer Tests in the Punjab Region of West Pakistan*; US Government Printing Office: Washington, DC, USA, 1967.
67. Akhter, G.; Ge, Y.; Iqbal, N.; Shang, Y.; Hasan, M. Appraisal of Remote Sensing Technology for Groundwater Resource Management Perspective in Indus Basin. *Sustainability* **2021**, *13*, 9686.
68. Hargreaves, G.H.; Samani, Z.A. Estimating potential evapotranspiration. *J. Irrig. Drain. Div.* **1982**, *108*, 225–230.
69. Tan, C.; Yang, J.; Li, M. Temporal-spatial variation of drought indicated by SPI and SPEI in Ningxia Hui Autonomous Region, China. *Atmosphere* **2015**, *6*, 1399–1421.
70. Qaiser, G.; Tariq, S.; Adnan, S.; Latif, M. Evaluation of a composite drought index to identify seasonal drought and its associated atmospheric dynamics in Northern Punjab, Pakistan. *J. Arid. Environ.* **2021**, *185*, 104332.
71. Wang, Y.; Lv, J.; Hannaford, J.; Wang, Y.; Sun, H.; Barker, L.J.; Ma, M.; Su, Z.; Eastman, M. Linking drought indices to impacts to support drought risk assessment in Liaoning province, China. *Nat. Hazards Earth Syst. Sci.* **2020**, *20*, 889–906.
72. Parsons, D.J.; Rey, D.; Tanguy, M.; Holman, I.P. Regional variations in the link between drought indices and reported agricultural impacts of drought. *Agric. Syst.* **2019**, *173*, 119–129.
73. Anwar, A.A.; Bhatti, M.T. Pakistan's water apportionment Accord of 1991: 25 years and beyond. *J. Water Resour. Plan. Manag.* **2018**, *144*, 05017015.
74. Yu, H.; Zhang, Q.; Sun, P.; Song, C. Impact of droughts on winter wheat yield in different growth stages during 2001–2016 in Eastern China. *Int. J. Disaster Risk Sci.* **2018**, *9*, 376–391.
75. Hamal, K.; Sharma, S.; Khadka, N.; Haile, G.G.; Joshi, B.B.; Xu, T.; Dawadi, B. Assessment of drought impacts on crop yields across Nepal during 1987–2017. *Meteorol. Appl.* **2020**, *27*, e1950.
76. Lobell, D.B.; Asner, G.P. Climate and management contributions to recent trends in U. S. agricultural yields. *Science* **2003**, *299*, 1032–1032.
77. Liu, X.; Pan, Y.; Zhu, X.; Yang, T.; Bai, J.; Sun, Z. Drought evolution and its impact on the crop yield in the North China Plain. *J. Hydrol.* **2018**, *564*, 984–996.
78. Kim, W.; Iizumi, T.; Nishimori, M. Global patterns of crop production losses associated with droughts from 1983 to 2009. *J. Appl. Meteorol. Climatol.* **2019**, *58*, 1233–1244.
79. Miyan, M.A. Droughts in Asian least developed countries: Vulnerability and sustainability. *Weather. Clim. Extrem.* **2015**, *7*, 8–23.
80. Naz, F.; Dars, G.H.; Ansari, K.; Jamro, S.; Krakauer, N.Y. Drought trends in Balochistan. *Water* **2020**, *12*, 470.
81. Chandrasekara, S.S.; Kwon, H.-H.; Vithanage, M.; Obeysekera, J.; Kim, T.-W. Drought in South Asia: A review of drought assessment and prediction in South Asian countries. *Atmosphere* **2021**, *12*, 369.
82. Ahmed, K.; Shahid, S.; Chung, E.-S.; Ismail, T.; Wang, X.-J. Spatial distribution of secular trends in annual and seasonal precipitation over Pakistan. *Clim. Res.* **2017**, *74*, 95–107.
83. Moors, E.J.; Stoffel, M. Changing monsoon patterns, snow and glacial melt, its impacts and adaptation options in northern India: Synthesis. *Sci. Total Environ.* **2013**, *468–469*, S162–S167.
84. Van Loon, A.F.; Rangelcroft, S.; Coxon, G.; Werner, M.; Wanders, N.; Di Baldassarre, G.; Tjeldeman, E.; Bosman, M.; Gleeson, T.; Nauditt, A.N. Streamflow droughts aggravated by human activities despite management. *Environ. Res. Lett.* **2022**, *17*, 044059.
85. Ahmad, Z.; Hafeez, M.; Ahmad, I. Hydrology of mountainous areas in the upper Indus Basin, Northern Pakistan with the perspective of climate change. *Environ. Monit. Assess.* **2012**, *184*, 5255–5274.
86. Tjeldeman, E.; Hannaford, J.; Stahl, K. Human influences on streamflow drought characteristics in England and Wales. *Hydrol. Earth Syst. Sci.* **2018**, *22*, 1051–1064.
87. Wada, Y.; Van Beek, L.P.; Wanders, N.; Bierkens, M.F. Human water consumption intensifies hydrological drought worldwide. *Environ. Res. Lett.* **2013**, *8*, 034036.
88. Ashraf, M.; Arshad, A.; Patel, P.M.; Khan, A.; Qamar, H.; Siti-Sundari, R.; Ghani, M.U.; Amin, A.; Babar, J.R. Quantifying climate-induced drought risk to livelihood and mitigation actions in Balochistan. *Nat. Hazards* **2021**, *109*, 2127–2151.
89. Joodaki, G.; Wahr, J.; Swenson, S. Estimating the human contribution to groundwater depletion in the Middle East, from GRACE data, land surface models, and well observations. *Water Resour. Res.* **2014**, *50*, 2679–2692.
90. Zipper, S.C.; Keune, J.; Kollet, S.J. Land use change impacts on European heat and drought: Remote land-atmosphere feedbacks mitigated locally by shallow groundwater. *Environ. Res. Lett.* **2019**, *14*, 044012.
91. Van Huijgevoort, M.H.; Voortman, B.R.; Rijkema, S.; Nijhuis, K.H.; Witte, J.-P.M. Influence of climate and land use change on the groundwater system of the Veluwe, The Netherlands: A historical and future perspective. *Water* **2020**, *12*, 2866.
92. Latif, Y.; Ma, Y.; Ma, W. Climatic trends variability and concerning flow regime of Upper Indus Basin, Jehlum, and Kabul river basins Pakistan. *Theor. Appl. Climatol.* **2021**, *144*, 447–468.
93. Vörösmarty, C.J.; McIntyre, P.B.; Gessner, M.O.; Dudgeon, D.; Prusevich, A.; Green, P.; Glidden, S.; Bunn, S.E.; Sullivan, C.A.; Liermann, C.R. Global threats to human water security and river biodiversity. *Nature* **2010**, *467*, 555–561.
94. Lall, U.; Josset, L.; Russo, T. A snapshot of the world's groundwater challenges. *Annu. Rev. Environ. Resour.* **2020**, *45*, 171–194.
95. Lorenzo-Lacruz, J.; Morán-Tejeda, E.; Vicente-Serrano, S.M.; López-Moreno, J.I. Streamflow droughts in the Iberian Peninsula between 1945 and 2005: Spatial and temporal patterns. *Hydrol. Earth Syst. Sci.* **2013**, *17*, 119–134.
96. Ma, F.; Luo, L.; Ye, A.; Duan, Q. Drought characteristics and propagation in the semiarid Heihe River Basin in Northwestern China. *J. Hydrometeorol.* **2019**, *20*, 59–77.
97. Hao, Y.; Hao, Z.; Feng, S.; Zhang, X.; Hao, F. Response of vegetation to El Niño-Southern Oscillation (ENSO) via compound dry and hot events in southern Africa. *Glob. Planet. Chang.* **2020**, *195*, 103358.

98. Li, H.; Chen, H.; Wang, H. Effects of anthropogenic activity emerging as intensified extreme precipitation over China. *J. Geophys. Res. Atmos.* **2017**, *122*, 6899–6914.
99. Aadhar, S.; Mishra, V. On the occurrence of the worst drought in South Asia in the observed and future climate. *Environ. Res. Lett.* **2021**, *16*, 024050.
100. Regmi, H.R. *Drought Risk Management in Nepal*; SAARC Disaster Management Centre: New Delhi, India, 2010.
101. Ali, S.; Liu, Y.; Ishaq, M.; Shah, T.; Ilyas, A.; Din, I.U. Climate change and its impact on the yield of major food crops: Evidence from Pakistan. *Foods* **2017**, *6*, 39.
102. Qaisrani, Z.N.; Nuthammachot, N.; Techato, K. Drought monitoring based on Standardized Precipitation Index and Standardized Precipitation Evapotranspiration Index in the arid zone of Balochistan province, Pakistan. *Arab. J. Geosci.* **2021**, *14*, 11.
103. Carrão, H.; Naumann, G.; Barbosa, P. Mapping global patterns of drought risk: An empirical framework based on sub-national estimates of hazard, exposure and vulnerability. *Glob. Environ. Chang.* **2016**, *39*, 108–124.
104. Arshad, A.; Zhang, Z.; Zhang, W.; Gujree, I. Long-term perspective changes in crop irrigation requirement caused by climate and agriculture land use changes in Rechna Doab, Pakistan. *Water* **2019**, *11*, 1567.
105. Pokhrel, Y.; Felfelani, F.; Satoh, Y.; Boulange, J.; Burek, P.; Gädeke, A.; Gerten, D.; Gosling, S.N.; Grillakis, M.; Gudmundsson, L. Global terrestrial water storage and drought severity under climate change. *Nat. Clim. Chang.* **2021**, *11*, 226–233.
106. Tiwari, V.; Wahr, J.; Swenson, S. Dwindling groundwater resources in northern India, from satellite gravity observations. *Geophys. Res. Lett.* **2009**, *36*, L18401.
107. Rodell, M.; Velicogna, I.; Famiglietti, J.S. Satellite-based estimates of groundwater depletion in India. *Nature* **2009**, *460*, 999–1002.
108. Luo, Z.; Yao, C.; Li, Q.; Huang, Z. Terrestrial water storage changes over the Pearl River Basin from GRACE and connections with Pacific climate variability. *Geod. Geodyn.* **2016**, *7*, 171–179.
109. Salma, S.; Rehman, S.; Shah, M. Rainfall trends in different climate zones of Pakistan. *Pak. J. Meteorol.* **2012**, *9*, 37–47.
110. Ren, Y.-Y.; Ren, G.-Y.; Sun, X.-B.; Shrestha, A.B.; You, Q.-L.; Zhan, Y.-J.; Rajbhandari, R.; Zhang, P.-F.; Wen, K.-M. Observed changes in surface air temperature and precipitation in the Hindu Kush Himalayan region over the last 100-plus years. *Adv. Clim. Chang. Res.* **2017**, *8*, 148–156.
111. Hussain, J.; Khaliq, T.; Ullah, A.; Ahmed, I.; Srivastava, A.K.; Gaiser, T.; Ahmad, A. Effect of Temperature on Sowing Dates of Wheat under Arid and Semi-Arid Climatic Regions and Impact Quantification of Climate Change through Mechanistic Modeling with Evidence from Field. *Atmosphere* **2021**, *12*, 927.
112. Khan, A.; Ali, S.; Shah, S.A.; Khan, A.; Ullah, R. Impact of climate change on maize productivity in Khyber Pakhtunkhwa, Pakistan. *Sarhad J. Agric.* **2019**, *35*, 594–601.
113. Hatfield, J.L.; Prueger, J.H. Temperature extremes: Effect on plant growth and development. *Weather. Clim. Extrem.* **2015**, *10*, 4–10.
114. Shah, H.; Siderius, C.; Hellegers, P. Cost and effectiveness of in-season strategies for coping with weather variability in Pakistan's agriculture. *Agric. Syst.* **2020**, *178*, 102746.
115. Hussain, A.; Bangash, R. Impact of climate change on crops' productivity across selected agro-ecological zones in Pakistan. *Pak. Dev. Rev.* **2017**, *56*, 163–187.
116. Ahmad, Q.-A.; Biemans, H.; Moors, E.; Shaheen, N.; Masih, I. The Impacts of Climate Variability on Crop Yields and Irrigation Water Demand in South Asia. *Water* **2021**, *13*, 50.
117. Pan, J. Area delineation and spatial-temporal dynamics of urban heat island in Lanzhou City, China using remote sensing imagery. *J. Indian Soc. Remote Sens.* **2016**, *44*, 111–127.
118. Chen, X.-L.; Zhao, H.-M.; Li, P.-X.; Yin, Z.-Y. Remote sensing image-based analysis of the relationship between urban heat island and land use/cover changes. *Remote Sens. Environ.* **2006**, *104*, 133–146.